ADJUSTABLE STIFFNESS VIBRATION ISOLATOR/ABSORBER SYSTEM

by

Sergen Haydın

B.S., Mechanical Engineering, Boğaziçi University, 2017

Submitted to the Institute for Graduate Studies in
Science and Engineering in partial fulfillment of
the requirements for the degree of
Master of Science

Graduate Program in Department of Mechanical Engineering
Boğaziçi University

2021

ACKNOWLEDGEMENTS

I would like to express my sincere appreciation to my thesis supervisor, Prof. Çetin Yılmaz, who has the attitude of a genius: he convincingly guided and encouraged me to do the right thing even when the road got tough. He is an inspirational person with great ideas and working with him was an invaluable experience for me. The purpose of this project could not have been achieved without his persistent help.

I am very grateful to my friends Endeş, Doğuş, Gamze, Nisan and Şenkız for their valuable supports. I would also like to thank to my friends Oğuz, Pelin and Sedef, who were my comrades during the master's study. It would be much harder without their cooperation. I wish to express my deepest gratitude to my dear Sena. She encouraged me at every stage of my thesis and made me feel loved.

I wish to thank all the people whose assistance was a milestone in the completion of this project and to express my apologies for not being able to mention one by one in person.

Finally, I would like to thank my beloved family with all my heartfelt feelings. This accomplishment would not have been possible without their support and encouragement.

ABSTRACT

ADJUSTABLE STIFFNESS VIBRATION ISOLATOR/ABSORBER SYSTEM

A new vibration isolator/absorber system with adjustable stiffness is developed and studied in this thesis. If this system is used in the load path between the excitation source and the receiver object, then it can be treated as a variable stiffness isolator. On the other hand, if it is attached on the receiver object, then it can work as a dynamic vibration absorber with variable natural frequency. The designed system consists of two main parts; axially loaded beams and quasi-zero stiffness mechanism. To create axial load on the beams, the quasi-zero stiffness mechanism is connected to the beams via a wire. As the axial force on the beams increases, the natural frequency of the system decreases. However, a large axial force is needed to significantly decrease the natural frequency of the system. With the help of the quasi-zero stiffness mechanism, this adjustment process can be done with almost zero effort. The quasi-zero stiffness mechanism consists of negative and positive stiffness elements. Negative stiffness is obtained using bistable buckled beams while positive stiffness is provided by a helical compression spring. Both analytical and finite element studies are provided for stiffness and natural frequency calculations. Moreover, the system is manufactured and examined experimentally. It is shown that analytical, numerical and experimental results are close. The system can be tuned with small effort and its natural frequency can be adjusted between 3.4 Hz and 16.4 Hz. Hence, the stiffness of the system can vary more than 20 times.

ÖZET

AYARLANABİLİR DİRENGENLİKLİ TİTREŞİM YALITIMI/YUTUCUSU SİSTEMİ

Bu tez çalışmasında ayarlanabilir direngenlikli yeni bir titreşim yalıtımı/yutucusu sisteminin tasarımı ve analizi yapılmıştır. Bu sistem, uyarı kaynağı ile alıcı nesne arasındaki yük yolunda kullanılıyorsa, değişken direngenlikli izolatör olarak ele alınabilir. Öte yandan, bu sistem alıcı nesneye takılırsa, değişken doğal frekanslı dinamik titreşim yutucusu olarak çalışabilir. Tasarlanan sistem iki ana bölümden oluşmaktadır; eksenel yüklenmiş kirişler ve yarı sıfır direngenlik mekanizması. Kirişler üzerinde eksenel yük oluşturmak için yarı sıfır direngenlik mekanizması bir tel ile kirişlere bağlanmıştır. Kirişler üzerindeki eksenel kuvvet arttığında sistemin doğal frekansı azalmaktadır. Bununla birlikte, sistemin doğal frekansını önemli ölçüde azaltmak için büyük bir eksenel kuvvet gereklidir. Yarı sıfır direngenlik mekanizması yardımıyla bu ayarlama işlemi neredeyse sıfır efor harcanarak yapılabilmektedir. Yarı sıfır direngenlik mekanizması negatif ve pozitif direngenlik elemanlarından oluşmaktadır. Negatif direngenlik, çift kararlı yapıya sahip burkulmuş kirişler kullanılarak; pozitif direngenlik, helisel basma yayından elde edilmiştir. Direngenlik ve doğal frekans hesaplamaları için hem analitik hem de sonlu eleman çalışmaları yapılmıştır. Ayrıca sistem deneysel olarak üretilmiş ve incelenmiştir. Analitik, sayısal ve deneysel sonuçların birbirine yakın olduğu gösterilmiştir. Sistem küçük bir eforla ayarlanabilmekte ve doğal frekansı 3.4 Hz ile 16.4 Hz arasında ayarlanabilmektedir. Dolayısıyla, sistemin direngenliği 20 kattan fazla değişebilmektedir.

TABLE OF CONTENTS

ACKNOWLEDGEMENTS iii
ABSTRACT iv
ÖZET v
LIST OF FIGURES vii
LIST OF TABLES xi
LIST OF SYMBOLS xii
LIST OF ACRONYMS/ABBREVIATIONS xiv
1. INTRODUCTION 1
1.1. Research Objective and Motivation 2
1.2. Quasi-Zero Stiffness (QZS) Mechanisms 3
1.3. Literature Review 5
2. THEORETICAL BACKGROUND AND DESIGN STAGES 9
2.1. Design Stages 9
2.1.1. Axially Loaded Beams 9
2.1.2. Quasi-Zero Stiffness Mechanism 17
2.1.2.1. Negative Stiffness Element 17
2.1.2.2. Positive Stiffness Element 23
2.1.3. Complete Design 28
3. EXPERIMENTAL RESULTS AND DISCUSSION 31
4. CONCLUSION 41
REFERENCES 42
APPENDIX A: TECHNICAL DRAWINGS 49
APPENDIX B: COPYRIGHTS 56

LIST OF FIGURES

Figure 1.1. Single degree of freedom mass-spring system. 1

Figure 1.2. Schematic representation of the simplest quasi-zero stiffness mechanism 4

Figure 1.3. Force-displacement curve of the QZS mechanism 5

Figure 1.4. The nonlinear isolator consisting of a linear isolator and the negative stiffness corrector. (a) With load balanced at the minimum stiffness point; and (b) with a distuning load (overload). 6

Figure 2.1. Clamped-roller beam deflection. 10

Figure 2.2. 3D view of the axially loaded beams. 13

Figure 2.3. (a) Schematic representation of axially loaded beams. (b) Idealized boundary conditions of axially loaded beams. 13

Figure 2.4. P_{cr}/P^*_{cr} versus l_w/l_b 16

Figure 2.5. Front view of negative stiffness element. 18

Figure 2.6. Force-displacement graph for a curved beam whose second buckling mode is constrained. 20

Figure 2.7. Apex height for the curved beam. 20

Figure 2.8. Force-displacement graph for the designed curved beam. 21

Figure 2.9. FEM model of the negative stiffness elements. 22

Figure 2.10. Force-displacement graph for the FEM model. 23

Figure 2.11. Helical compression spring with elliptical cross section. 24

Figure 2.12. FEM model of the helical spring with elliptical cross section. . . . 25

Figure 2.13. Force-displacement graph for FEM solution of the helical compression spring with elliptical cross section. 25

Figure 2.14. Front view of adjustable stiffness vibration isolator/absorber system: 1 - Helical spring, 2 - Spring cover plate, 3 - Negative stiffness beams, 4 - Adjustment nut, 5 - Tension wire, 6 - Parallel beam set 28

Figure 2.15. (a) Isometric view of the adjustable stiffness vibration isolator/ absorber system. (b) Side view of the adjustable stiffness vibration isolator/absorber system. 29

Figure 3.1. The experimental setup showing the prototype (1) that is compressed by the universal testing machine (2), meanwhile the laser vibrometer (3) measures the vibration velocity of the block at the free end of the parallel beam set. The vibration data is obtained through the data acquisition system (4) and the data is analyzed by the computer (5). 32

Figure 3.2. Compression test of negative stiffness element. 33

Figure 3.3. Experimental force-displacement graph of the negative stiffness element. 33

Figure 3.4. Compression test of quasi-zero siffness system. 34

Figure 3.5. Experimental force-displacement graph of the quasi-zero stiffness system. 34

Figure 3.6. (a) Experimental velocity-time graph of the block at the free end of the parallel beam set in the quasi-zero stiffness system. (b) The corresponding force-time graph that is required to adjust the system. 35

Figure 3.7. Compression test of helical spring. 36

Figure 3.8. Experimental force-displacement graph of the helical spring. . . . 37

Figure 3.9. Natural frequency of the system for different compression values. . 37

Figure 3.10. Analytical and experimental results for natural frequency. 38

Figure 3.11. Analytical, finite element and experimental results for the helical spring. 39

Figure 3.12. Analytical, finite element and experimental results for negative stiffness element. 39

Figure A.1. Axially loaded beams. 49

Figure A.2. Spacer between the axially loaded beams. 50

Figure A.3. Negative stiffness element. 50

Figure A.4. Part between positive stiffness element and negative stiffness element. 51

Figure A.5. Top and bottom holders of axially loaded beams. 51

Figure A.6. Wire holder. 52

Figure A.7. Fixed frame. 52

Figure A.8. Connector with elliptical hole. 53

Figure A.9. Side bottom connector pieces. 53

Figure A.10. Side middle pieces. 54

Figure A.11. Side top pieces. 54

Figure A.12. Center bottom piece. 55

Figure A.13. Front view of final design. 55

Figure B.1. Copyright 1 56

Figure B.2. Copyright 2 57

Figure B.3. Copyright 3 58

LIST OF TABLES

Table 2.1. The first transverse natural frequency of the system for different compression values in mm. 30

LIST OF SYMBOLS

A	First constant of differential equation solution
A_w	Cross sectional area of wire
a	Semi-minor axis length of elliptical cross section
B	Second constant of differential equation solution
b	Semi-major axis length of elliptical cross section
b_b	Width of axially loaded beams
b_n	Width of negative stiffness beams
C	Third constant of differential equation solution
c	Viscous damping
D	Fourth constant of differential equation solution
d_{end}	Center displacement at where force is zero
d_{mid}	Center displacement at where force changes its sign
d_{min}	Center displacement at where force is minimum
d_{top}	Center displacement at where force is maximum
E_b	Elastic modulus of axially loaded beams
E_n	Elastic modulus of negative stiffness beams
E_w	Elastic modulus of wire
F_{top}	Maximum force of negative stiffness element
F_{bot}	Minimum force of negative stiffness element
G	Shear modulus of the helical spring
h	Apex height
I_b	Inertia of axially loaded beam
I_n	Inertia of negative stiffness beam
i	Mode number
k_b	Linear stiffness of a beam
$k_{p(Anal)}$	Analytically calculated positive stiffness of helical spring
$k_{p(Exp)}$	Experimentally obtained positive stiffness of helical spring
$k_{p(FEM)}$	Positive stiffness of helical spring for the FEM solution

$k_{pt(Anal)}$	Total effective positive stiffness
$k_{n(Anal)}$	Analytically calculated negative stiffness
$k_{n(Exp)}$	Experimentally obtained negative stiffness
$k_{n(FEM)}$	Negative stiffness for the FEM solution
$k_{w(Anal)}$	Analytically calculated axial stiffness of wire
l_b	Initial length of axially loaded beams
l_n	Initial length of negative stiffness beams
l_w	Active length of wire
l_{wf}	Full length of wire
M	Constant of differential equation solution
N_i	Eigenvalues of normalized axial force
n_a	Active coil number of helical spring
P	Axial force
P_{cr}	Critical buckling force
P_n	Axial force on negative stiffness beam
R	Mean coil radius of helical spring
r_w	Radius of wire
t_b	Thickness of axially loaded beams
t_n	Thickness of negative stiffness beams
$w(x)$	Displacement of negative stiffness beams
x_e	Equilibrium position
$y(x)$	Displacement of axially loaded beams

γ	Constant in the differential equation of axially loaded beams
δ	Tip displacement of axially loaded beams
λ_i	Non-dimensional frequency parameter
ω_1	Natural frequency of a beam in the presence of axial load
ω_b	The first transverse natural frequency of a beam

LIST OF ACRONYMS/ABBREVIATIONS

3D	Three Dimensional
CAE	Computer Aided Engineering
DOF	Degree of Freedom
DVA	Dinamic Vibration Absorber
FEM	Finite Element Method
Hz	Hertz
MRE	Magnetorheological Elastomer
QZS	Quasi-Zero Stiffness
SAIVS	Semi-Active and Independently Variable Stiffness

1. INTRODUCTION

Vibration or oscillation can be described as any motion that repeats itself after an interval of time. After the discovery of first musical instruments, probably drums or whistles, people became interested in vibration [1]. The simplest example for vibration or oscillation is a single degree of freedom mass-spring system (Figure 1.1). The system contains a mass block and a single spring. If the mass is displaced a certain distance from the equilibrium, the spring will have some potential energy, which will be converted into kinetic energy as the mass gains speed. Then, the mass will overshoot the rest position and deflect the spring in the opposite direction. It will then decelerate to stop at the other extreme of its displacement range where the spring will again push the mass towards the equilibrium point. The same process occurs repeatedly with the energy sloshing back and forth between the mass block and the spring, from potential energy in the spring to kinetic energy in the mass and back [2].

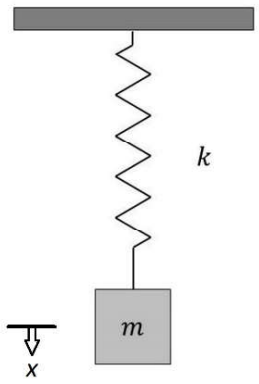


Figure 1.1. Single degree of freedom mass-spring system.

A vibration isolation system is used to eliminate undesirable vibrations at different frequencies by modifying the vibration transmissibility. Using a vibration isolation system is a practical solution in cases where transmission paths for vibrational energy can be identified and physically modified [3].

There are different types of passive vibration isolation systems. Helical or leaf springs behave linearly for moderate amplitudes and they are commonly used for vibration isolation [4–7]. Wire-rope isolators are used in passive vibration isolation systems and they exhibit non-linear stiffness behaviour [8–10]. Besides metal isolators, rubber vibration isolators are widely used in mechanical systems. The high resilience and energy dissipation capacity of rubber vibration isolators are the distinguishing characteristics that make them effective for controlling vibration [11, 12]. Unlike deformable solid structures, in air springs stiffness and/or the equilibrium position can be adjusted by controlling air pressure and volume. Air spring systems are used in luxury vehicles or heavy vehicles [13–15].

Passive dynamic vibration absorbers have been widely used to reduce vibration generated by seismic excitations, wind, maritime waves excitation, unbalanced rotating equipment, dynamic vibration caused by vehicle traffic, and other sources. Multiple DVAs arranged in parallel or series have improved the dynamic performance and robustness of the classical DVA [16–21]. Passive DVAs are effective only when the tuning and damping are proper for specific operating and environmental conditions. Because these conditions often change with time, passive DVAs may become mistuned and lose their effectiveness [22]. To that end, active or adaptive DVAs can be utilized.

1.1. Research Objective and Motivation

Undesirable vibrations have negative effect on all machinery equipment. In addition to that, noise level of machines increases due to these vibrations. Vibration isolation systems are widely used to protect systems from detrimental effects of vibration. When the excitation frequency changes, the isolation performance of a passive vibration isolation system changes.

The main aim of this thesis is to design a vibration isolator/absorber system with adjustable stiffness. The stiffness in most of existing vibration isolation systems is usually of fixed value. However, the disturbance frequency may change with time.

This problem can be solved by designing an adjustable vibration isolator that can respond to changes in excitation frequency. Moreover, if a dynamic vibration absorber with variable stiffness can be designed, then it can be tuned to various excitation frequencies.

The main motivation of this study is to design a novel adjustable stiffness system which can be used as a vibration isolator or vibration absorber. There are several adjustable stiffness or variable stiffness systems in the literature. Unlike the examples in the literature, the stiffness change will be done with almost zero effort. To achieve this, negative stiffness elements will be used. Another important feature of the design is that the response time will be very small. Hence, the natural frequency of the system will be changed in a wide frequency range very quickly and easily.

1.2. Quasi-Zero Stiffness (QZS) Mechanisms

The level of vibration in various machines and devices is one of the indicators of quality and reliability. Vibration protecting systems, which are placed between a vibration source and an isolated object, are frequently used to protect objects from dynamic disturbances. QZS mechanisms are usually created by combining a positive stiffness element with a negative stiffness element. The natural frequency and load bearing capability of vibration protecting systems are the most essential features. By lowering the natural frequency of the vibration protecting system, effectiveness of vibration isolation is greatly improved. However, without increasing overall dimensions, the load bearing capacity of a linear vibration protecting system cannot be maintained. This contradiction between load bearing capacity and natural frequency is eliminated with quasi zero stiffness [23].

There are many QZS mechanisms in the literature with different configurations. Examples of these mechanisms are using nonlinear features such as spring direction or buckling to create a negative stiffness effect. One of the simplest examples of these mechanisms consists of two oblique springs and one vertical spring. When the mech-

anism is loaded with an appropriately sized mass, the oblique springs are compressed so that they are in a horizontal position and the static load is carried by the vertical spring. This is the static equilibrium position, and the primary concern is the motion around that position. If the springs system is used in this way, oblique springs serve as a negative stiffness element in the vertical direction and resist the positive stiffness of the vertical spring.

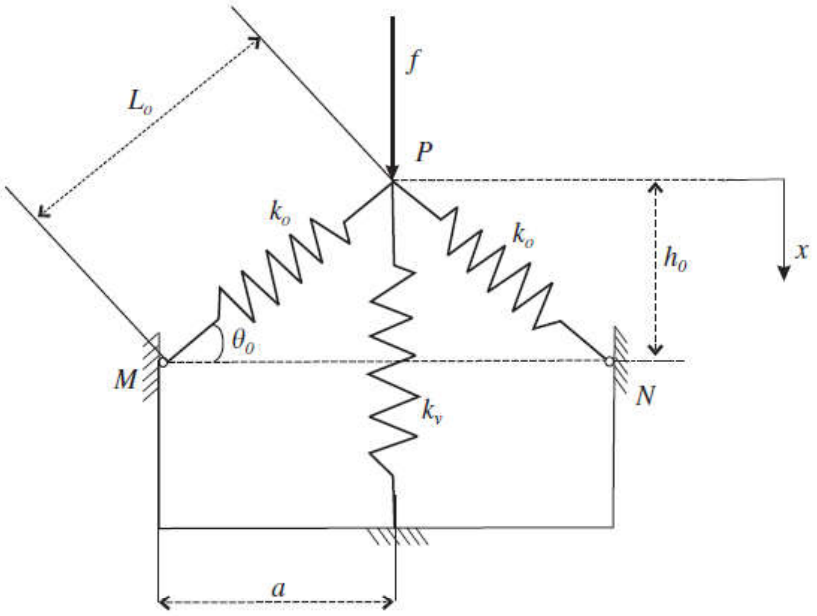


Figure 1.2. Schematic representation of the simplest quasi-zero stiffness mechanism [24].

Force-displacement curve for a typical system is nonlinear. Here, stiffness, which is the slope of the curve, varies as a function of displacement. For the particular case shown in Figure 1.2, the geometry and stiffness are chosen to make the stiffness zero at the static equilibrium position, x_e. The disadvantage of this special case is that when moving away from the equilibrium position, the system becomes stiffer than the vertical spring alone [24].

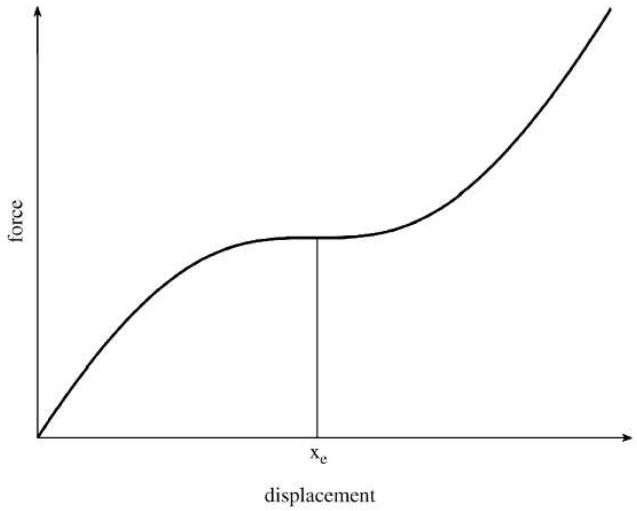


Figure 1.3. Force-displacement curve of the QZS mechanism [24].

1.3. Literature Review

Nonlinear isolators have attracted growing interest in recent years, as they have some advantages compared to linear ones in some respects. There are two types of elements which can essentially describe a vibration isolator: damping and stiffness. Both the nonlinearities in damping and stiffness are considerably explored in order to enhance the efficiency of isolation. Stiffness plays a very important role in vibration isolation, because it determines the isolator's bandwidth starting frequency. The dilemma is that in order to achieve a broader frequency range of isolation, the stiffness must be decreased which would ultimately result in a very large static displacement for a linear isolator. The negative stiffness mechanism was raised to minimize the impact of this problem and to achieve isolation of ultra-low frequency vibrations [25]. Huang et al. [25] studied a nonlinear isolator that employs an Euler beam as the negative stiffness corrector theoretically and experimentally. A linear isolator modeled by a linear stiffness, k, and viscous damping, c, is added parallel to the corrector. It is found that if vibration transmissibility is considered, a nonlinear isolator has a wider isolation frequency region compared to a linear one since the negative stiffness corrector reduces the overall stiffness of the linear isolator. Nevertheless, the experimental results show

that due to the effect of the added damping, the attenuation performance of the nonlinear isolator in the higher frequency range is degraded a bit. A feasible and efficient way to make this kind of nonlinear isolator work better is to reduce the added damping to the device and to use it in applications where the amplitude of excitation is not too large [25].

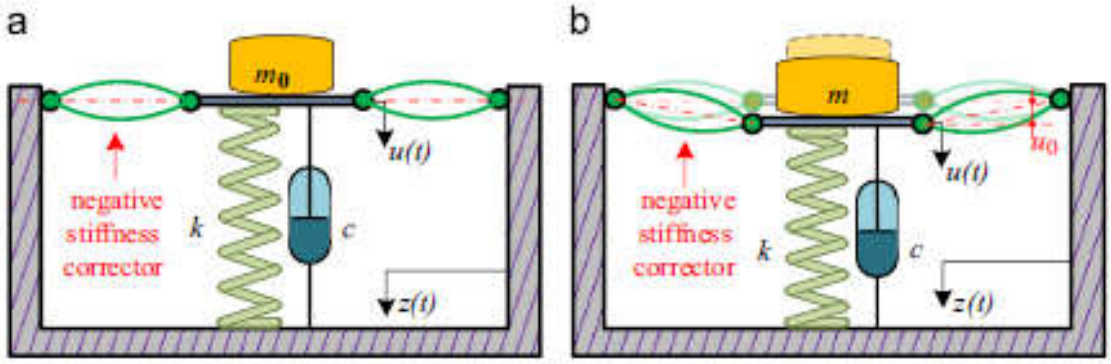


Figure 1.4. The nonlinear isolator consisted of a linear isolator and the negative stiffness corrector composed of buckled beams. (a) With load balanced at the minimum stiffness point; and (b) with a distuning load (overload) [25].

In general, a dynamic vibration absorber (DVA) can be viewed as a device attached to a structure designed to counteract its vibrations. The attenuation of the vibration happens when the natural frequency of DVA coincides with the excitation frequency [26, 27]. A tuned DVA design is studied in [28], which uses a string under variable tension with a central mass attachment as an undamped DVA. To make the system adaptive, a tuning controller is used. Additionally, a negative stiffness mechanism is employed to reduce the adaptation effort without losing the tuning speed. With the assistance of this method, the tuning actuator's force output requirement is reduced to almost zero. With the purpose of modularity, a microcontroller based control system is designed. A tuning algorithm, which determines the string tension, depending on the amplitude and frequency of the protected system vibration, is implemented in this microcontroller. It has been shown in the forced vibration tests that the designed system can significantly reduce the vibration level of the protected structure over the frequency range of the operations. Natural frequency of the DVA can be adjusted between 9.92 Hz and 19.68 Hz [28].

According to control principle a vibration isolation system can be classified as active, passive or semi-active (adaptive) [29]. Franchek et al. [30] presented a robust tuning strategy for adaptive control. In this study, a tunable stiffness vibration absorber was constructed. A mechanism is introduced, which is used to change the stiffness of a helical spring by adjusting the number of active coils. The frame for the absorber consists of a base and two end plates. A guide rod is mounted on the end plates and acts as a reference for the cylindrical weight. A circular bearing is pressed down into the middle of the mass to reduce frictional losses. A helical spring is attached by a locking plate to the mass. Threaded through a collar plate, this spring has a spur gear attached to its free end. The collar plate is constructed such that the spring coils are separated from the rest of the spring between the mass and its corresponding face. So it is possible to adjust the effective number of coils by rotating the helical spring, however, the absorber is limited to the frequency range between 5.9 Hz and 7.7 Hz [30].

Another study on semi-active vibration absorbers is by Ghorbani-Tanha et al. [31]. In the proposed variable stiffness device, the system stiffness can be changed with the help of a mechanism that can rotate a flexible beam. This device is able to smoothly alter its stiffness between minimum and maximum levels by using the variations in the second moment of area of the beam as it rotates around a normal axis that passes through its centroid. Using the principle of unsymmetrical beam bending, theoretical expressions for the change in system stiffness as a function of rotation angle are developed. The stiffness of the system can vary 49 times. It takes 1.6 seconds for the system to reach from minimum stiffness to maximum stiffness.

In [32], a control device which effectively isolates building vibrations is introduced. Power requirement of the device is low and manufacturing process is cheap. SAIVS device can change its stiffness continuously and smoothly. Maximum and minimum stiffness values are designed. It consists of four springs and a telescoping tube. It maintains the structure in a non-resonant vibration state under unpredictable and complex disturbances like earthquakes and windstorms. The natural frequency range of the device can be changed between 0.71 Hz and 1.89 Hz.

In [33], an actuator with adjustable stiffness is presented. This device is designed for robot arms. In [34], a tunable vibration isolator with variable stiffness and damping is provided. Leaf springs are used in this isolator design. Parallel curved beams are used in [35], in order to change the stiffness of the system. It works between 36-56 Hz. In [36], a QZS vibration isolator using flexure-based spring mechanism is provided. In [37], a compact 6 degree of freedom(DOF) passive isolation system is described. In [38], a high-static-low-dynamic stiffness isolator using linear springs and magnets are provided. Another vibration isolator design using magnets is provided in [39]. In [40], behavior of negative stiffness elements is studied. In [41], buckled struts are used for the purpose of vibration isolation. In [42], a vehicle driver vibration isolation system is presented. In order to minimize the fundamental frequencies springs with negative stiffness is used. Another vehicle seat suspension system is described in [43], magnetorheological elastomer(MRE) isolator is used in the design. A semi-active controller is proposed and better vibration reducing performance than conventional on-off control is achieved. In [44], a low frequency flexible platform as a vibration isolator for reaction wheel assemblies is validated experimentally. In [45], an inerter based active vibration isolation system is presented. In [46], a magnetorheological fluid-based variable stiffness and damping isolator for vibration suppression is provided. A low frequency vibration isolator mechanism with adjustable configurative parameter to change of the weight of the isolated object is studied in [47].

When all the studies in the literature are investigated, it is seen that there is not a variable stiffness system, whose stiffness can be changed with almost zero effort in wide range in very short time. Hence, this thesis focuses on developing such a system.

2. THEORETICAL BACKGROUND AND DESIGN STAGES

In this section of the thesis, the design stages of the adjustable stiffness system will be introduced. Analytical model and finite element model of the system will be compared.

2.1. Design Stages

The system is composed of two main parts, axially loaded beams and quasi-zero stiffness mechanism. The principle of buckling of beams is used to change natural frequency of the axially loaded beams in the system. The quasi-zero stiffness part of the system is used to change the natural frequency of the system quickly and with almost zero effort.

2.1.1. Axially Loaded Beams

A tensile load that is applied axially to a beam raises the beam's first transverse natural frequency. On the other hand, if compressive axial load is applied to the beam, the first transverse natural frequency decreases. The first transverse natural frequency (ω_1) of a beam in the presence of axial load can be written as

$$\omega_1 = \beta_1^2 \sqrt{\frac{E_b I_b}{\rho_b A_b}} \sqrt{(1 + \frac{P}{P_{cr}})} \tag{2.1}$$

where β_1 is a constant that depends on the boundary conditions; E_b is the elastic modulus, ρ_b is the density, A_b is the area, I_b is the second moment of area of the beam; P is the applied axial force (plus for tensile force and minus for compressive force); P_{cr} is the first critical axial compressive load to buckle the beam [48]. If a compressive force, P, is gradually increased, a situation is reached in which the flat equilibrium

shape becomes unstable and a small lateral force produces a deflection that does not disappear when the lateral force is removed. The critical load is defined as the axial compressive force sufficient to hold the beam in such a slightly bent shape [49].

In order to achieve the desired stiffness and load carrying capacity, more than one beam must be used in the system. Parallel beam configuration will be used to ensure system stability.

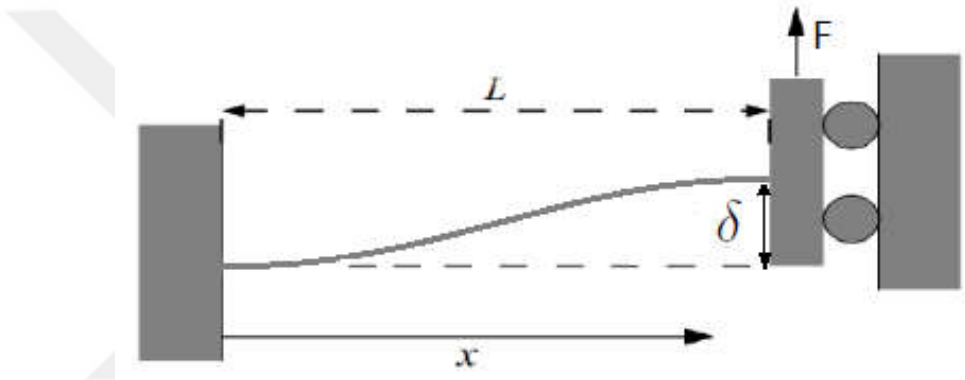


Figure 2.1. Clamped-roller beam deflection.

According to the Euler-Bernoulli Beam Theory, lateral stiffness of a beam with clamped-roller boundary conditions as shown in Figure 2.1. Lateral stiffness of a beam can be calculated as

$$k_b = \frac{F}{\delta} = \frac{12 E_b I_b}{l_b^3} \tag{2.2}$$

and the second moment of area of the beam with rectangular cross section can be calculated as

$$I_b = \frac{1}{12} b_b t_b^3 \tag{2.3}$$

where δ is the deflection of the beam, F is the transverse force on the free end, l_b is the length of the beam, E_b is the elastic modulus of the beam, I_b is the inertia of the beam with rectangular cross section, b_b is width of the beam and t_b is thickness of the beam [50].

The maximum bending moment in a beam is

$$M = \frac{F l_b}{2}. \tag{2.4}$$

When Equation (2.2) is used in Equation (2.4), bending moment can be obtained as

$$M = \frac{6\delta E_b I_b}{l_b^2}. \tag{2.5}$$

So, the maximum stress can be found as

$$\sigma = \frac{M t_b}{2 I_b} = \frac{3\delta E_b t_b}{l_b^2}. \tag{2.6}$$

Hence, for a given yield strength, maximum value of δ can be determined as

$$\delta_{max} = \frac{\sigma_y l_b^2}{3 E_b t_b}. \tag{2.7}$$

As this beam is to be used for in a vibration isolator or absorber, a large δ_{max} is desirable. Spring steel can be used to have a high value of σ_y. Although increasing l_b is beneficial, it cannot be increased very much to have a compact design. Finally, t_b can be decreased to have a large δ_{max}. But, in that case k_b will be small and the beam cannot support large loads. In order to overcome these issues, parallel beams are used.

There are 8 beams on each side and a wire at the center can provide compressive axial load on each beam once it is pulled from its free end.

The targeted lateral stiffness of the parallel beam set with 16 beams ($n_b = 16$) is 1600N/mm, so the parameters of the beams are selected as E_b=200 GPa, b_b=18.5 mm, t_b=0.3 mm, l_b=100 mm. Then, these parameters can be used in Equation (2.2) and Equation (2.3) to find k_b as

$$k_b = 1598.4 \text{ N/m}. \tag{2.8}$$

The first transverse natural frequency of the parallel beam set when there is no axial load can be calculated as

$$w_b = \frac{1}{2\pi}\sqrt{\frac{k_b}{m}}. \tag{2.9}$$

The natural frequency of the system in the no axial load case is targeted to correspond to 1000 rpm, hence w_b is selected as 16.66 Hz. According to Equation (2.9), m is determined as 146 grams. Moreover, when there is axial load on the paralel beam set, then the first natural frequency can be calculated as

$$w_b = \frac{1}{2\pi}\sqrt{\frac{k_b}{m}}\sqrt{1 + \frac{P}{P_{cr}}}. \tag{2.10}$$

Therefore, by increasing the compressive force on the beams, the natural frequency can correspond to rpms between 0 and 1000.

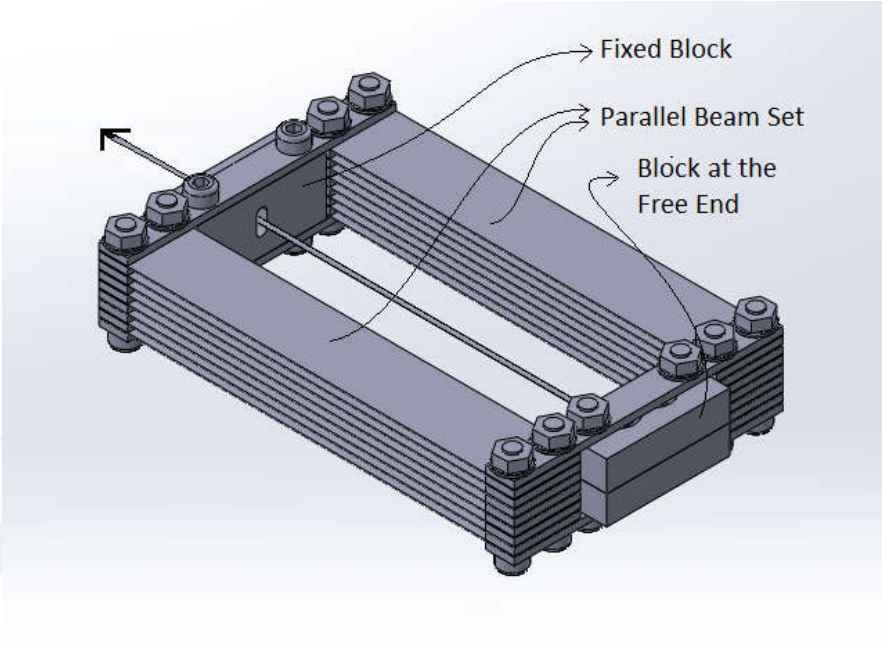


Figure 2.2. 3D view of the axially loaded beams.

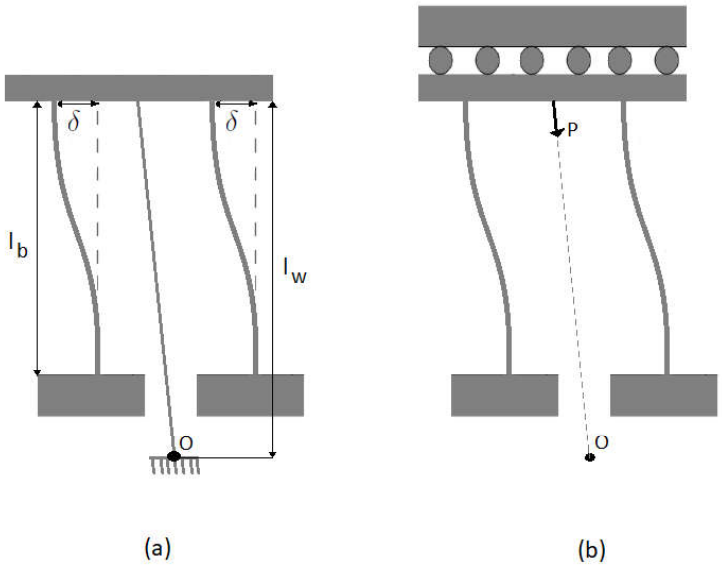


Figure 2.3. (a) Schematic representation of axially loaded beams. (b) Idealized boundary conditions of axially loaded beams.

An axial compressive load is needed to reduce the natural frequency of the beams. A wire is used to apply this force. Each beam is clamped from one end and there is roller boundary at the other end. Critical loads of beams can be determined as

$$E_b I_b \frac{d^4y}{dx^4} + P\frac{d^2y}{dx^2} = 0. \tag{2.11}$$

Equation (2.11) can be written in more compact form by defining γ^2 as

$$\gamma^2 = \frac{P}{E_b I_b}. \tag{2.12}$$

Consequently, Equation (2.11) can be written as

$$\frac{d^4y}{dx^4} + \gamma^2\frac{d^2y}{dx^2} = 0. \tag{2.13}$$

The general solution of this equation is

$$y(x) = A\sin(\gamma x) + B\cos(\gamma x) + Cx + D. \tag{2.14}$$

The constants A, B, C, D in this equation can be found from the following boundary conditions. Boundary conditions can be written as

$$y = \frac{dy}{dx} = 0 \quad at \quad x = 0, \tag{2.15}$$

$$\frac{d^3y}{dx^3} + \gamma^2\frac{dy}{dx} = \gamma^2\frac{\delta}{l_w} \quad and \quad \frac{dy}{dx} = 0 \quad at \quad x = l_b \tag{2.16}$$

where δ is the deflection of the beam at roller end boundary condition and l_w is the length of the wire. Equations (2.15) and (2.16) can be used in Equation (2.14) to find A, B, C and D as

$$A = -\frac{\delta}{\gamma l_w}, B = \frac{\delta}{\gamma l_w}\left[\frac{1 - cos(\gamma l_b)}{sin(\gamma l_b)}\right], C = \frac{\delta}{l_w}, D = -\frac{\delta}{\gamma l_w}\left[\frac{1 - cos(\gamma l_b)}{sin(\gamma l_b)}\right]. \tag{2.17}$$

When the constants in Equation (2.17) is used in Equation (2.14), deflection of the beam can be obtained as

$$y(x) = \frac{\delta}{\gamma l_w}\left[\frac{(1 - \cos(\gamma l_b))(\cos(\gamma x) - 1)}{\sin(\gamma l_b)} - \sin(\gamma x) + \gamma x\right]. \tag{2.18}$$

Notice that $y(l_b) = \delta$ (see Fig. 2.3). Once, this condition is used in Equation (2.18), the characteristic equation of this beam can be determined as

$$\gamma l_b \left(1 - \frac{l_w}{l_b}\right) = \frac{2 - 2\cos(\gamma l_b)}{\sin(\gamma l_b)}. \tag{2.19}$$

Equation (2.19) can be solved for γl_b iteratively by using given l_w/l_b ratios. Once γl_b is determined for a specific l_w/l_b ratio, Equation (2.12) can be used to find the critical buckling force $P_{cr}(l_w/l_b)$. When l_w/l_b approaches infinity, then the classical buckling formula in the presence of an external force is obtained for clamped-roller boundary conditions as

$$P^*_{cr} = \frac{\pi^2 E_b I_b}{l_b^2}. \tag{2.20}$$

Notice for large l_w/l_b values, P_{cr}/P^*_{cr} approaches 1 as expected. Moreover, when l_w/l_b=1, P_{cr}/P^*_{cr}=4. In other words, when $l_w = l_b$, P_{cr} equals to the classical buckling force in the presence of an external force is obtained for clamped-clamped boundary

conditions. In order to reduce the transverse stiffness of the roller end, the wire tension (P) should approach P_{cr}. In order to reduce the size of the system l_w should be made as small as possible. As l_w/l_b gets smaller P_{cr} gets larger. If P_{cr} is large, then it will be hard to reduce the transverse natural frequency by increasing the tension in the wire. To have a reasonable size and tension value, l_w/l_b can be chosen between 1.5 and 2.

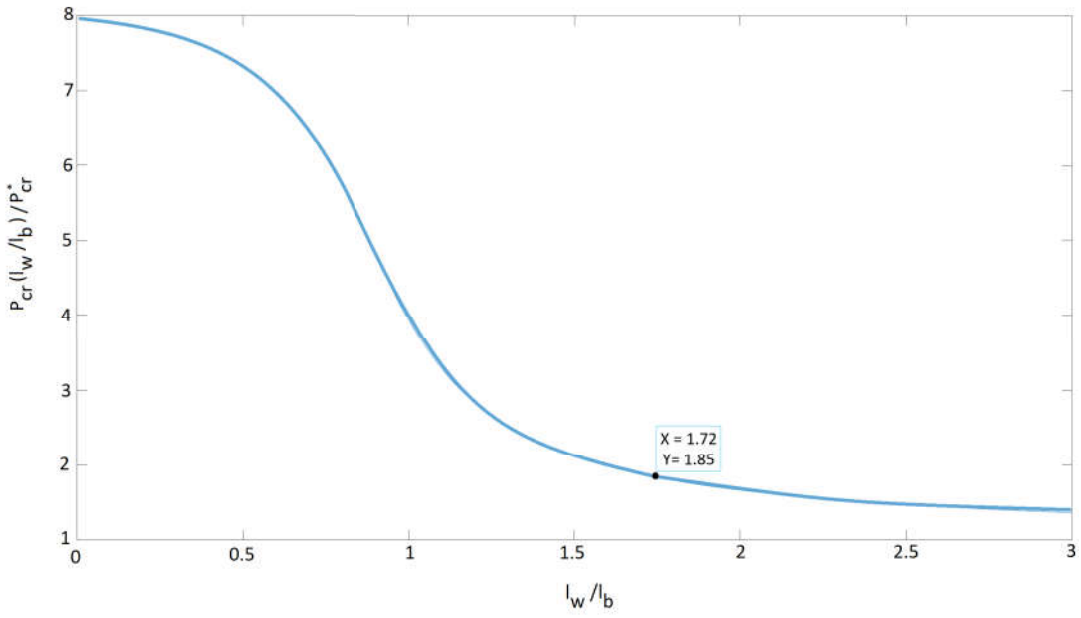


Figure 2.4. P_{cr}/P^*_{cr} versus l_w/l_b

In the design there are sixteen beams. The parameters of the beams were chosen as E_b=200 GPa, b_b=18.5 mm, t_b=0.3 mm, l_b= 100 mm. Moreover, l_w is chosen as 172 mm so, l_w/l_b=1.72. According to Figure 2.4, P_{cr}/P^*_{cr}=1.85. Since there are 16 beams, P_{cr} can be found as

$$P_{cr} = 16 \times \frac{1.85\pi^2 E_b I_b}{l_b^2}. \tag{2.21}$$

By inserting the parameters of the system in Equation (2.21), P_{cr} can be found as

$$P_{cr} = 243.2 \text{ N}. \tag{2.22}$$

Notice that P_{cr} is close to 240 N. Hence, if the positive stiffness is equal to 30 N/mm and the negative stiffness is equal to -30 N/mm in the quasi-zero stiffness system, then with 8 mm stroke, the beams in the parallel beam set can be almost buckled, which reduces the lateral natural frequency to zero (see Equation (2.10)). Moreover, by using lower stroke values, the lateral natural frequency can take any value between 0 Hz and 16.66 Hz.

2.1.2. Quasi-Zero Stiffness Mechanism

The axial compression load is applied to the parallel beam set by a wire. This wire is also connected to a quasi-zero stiffness mechanism. The purpose of using this quasi-zero stiffness mechanism is to change the natural frequency of the beams with almost zero effort. This mechanism consists of two main parts, the negative stiffness element and the positive stiffness element.

2.1.2.1. Negative Stiffness Element. Negative stiffness is an important way to improve vibration isolation. Although positive stiffness systems have increased resistance to deformation from externally applied forces, negative stiffness systems need lower levels of force with increasing displacement [51]. In the design, axially compressed buckled straight-beam mechanism is used as a negative stiffness element.

The negative stiffness mechanism design is inspired by buckled bistable straight-beam mechanisms, where a straight beam is compressed axially to buckle to stable positions on either side. It is critical to comprehend modeling of a curved-beam mechanism to model the buckling modes of the straight beam mechanism [52]. The beam equation that is describing a straight beam subjected to an axial load P_n can be found as

$$E_n I_n \frac{d^4 w}{dx^4} + P_n \frac{d^2 w}{dx^2} = 0 \tag{2.23}$$

where w is the lateral beam displacement, E_n is the elastic modulus of the negative stiffness beam material and I_n is the moment of inertia of the negative stiffness beam. The boundary conditions of clamped-clamped conditions of Equation (2.23) are

$$w(x) = \frac{dw}{dx} = 0 \quad at \quad x = 0 \quad and \quad x = l_n \tag{2.24}$$

where l_n is the length of the negative stiffness beam. Axial force is normalized by,

$$N^2 = \frac{P_n l_n^2}{E_n I_n}. \tag{2.25}$$

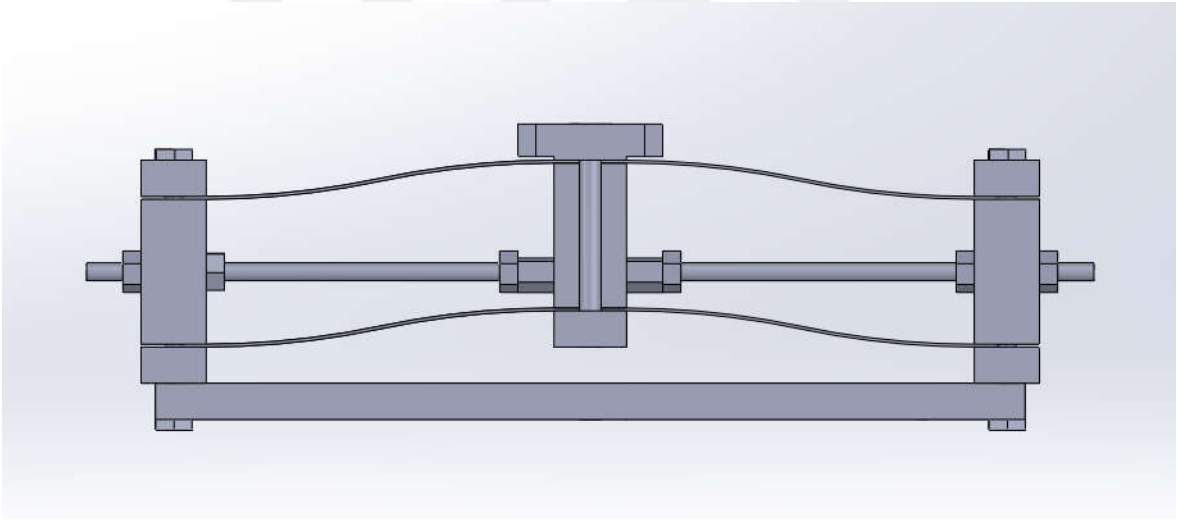


Figure 2.5. Front view of negative stiffness element.

To have non-zero solutions of this homogenous Sturm-Liouville problem, eigenvalues N_i must satisfy,

$$\sin\left(\frac{N_i}{2}\right)\left[\tan\left(\frac{N_i}{2}\right) - \frac{N_i}{2}\right] = 0. \tag{2.26}$$

Which allows two kinds of solution, namely

$$\left.\begin{aligned} w_i(x) &= M\left[1-\cos\left(N_i\frac{x}{l_n}\right)\right] \\ N_i &= (i+1)\pi \end{aligned}\right\} \quad \text{i=1,3,5...} \tag{2.27}$$

$$\left.\begin{aligned} w_i(x) &= M\left[1-2\frac{x}{l_n}-\cos\left(N_i\frac{x}{l_n}\right)+\frac{2\sin\left(N_i\frac{x}{l_n}\right)}{N_i}\right] \\ N_i &= 2.86\pi, 4.92\pi... \end{aligned}\right\} \quad \text{i=2,4,6...} \tag{2.28}$$

The above analysis provides an analytical basis for a buckling analysis. In the design, two parallel beams are used as negative stiffness elements. These beams are axially compressed to buckle in a vertical direction to achieve negative stiffness. Critical force for the beam with clamped-clamped boundary conditions is calculated as

$$P_{cr} = \frac{4\pi^2 E_n I_n}{l_n^2}. \tag{2.29}$$

Force-displacement relationship for the bistable buckled straight beam is examined in [52]. The lateral force that is applied to the center of the second-mode-constrained curved beam and the deflection of the beam center can be calculated as

$$\begin{aligned} F_{top} &= 740\frac{E_n I_n h}{l_n^3}, \\ F_{bot} &= 370\frac{E_n I_n h}{l_n^3}, \end{aligned} \tag{2.30}$$

$$\begin{aligned} d_{top} &= 0.16h, \\ d_{mid} &= \frac{4}{3}h, \\ d_{bot} &= 1.92h, \\ d_{end} &= 1.99h \end{aligned} \tag{2.31}$$

where l_n is the length of the negative stiffness beam, E_n is the elastic modulus of the negative stiffness beam, I_n is the second moment of area of the negative stiffness beam with rectangular cross section, h is the apex height. These parameters are valid for the apex height is greater than 6 times the beam thickness.

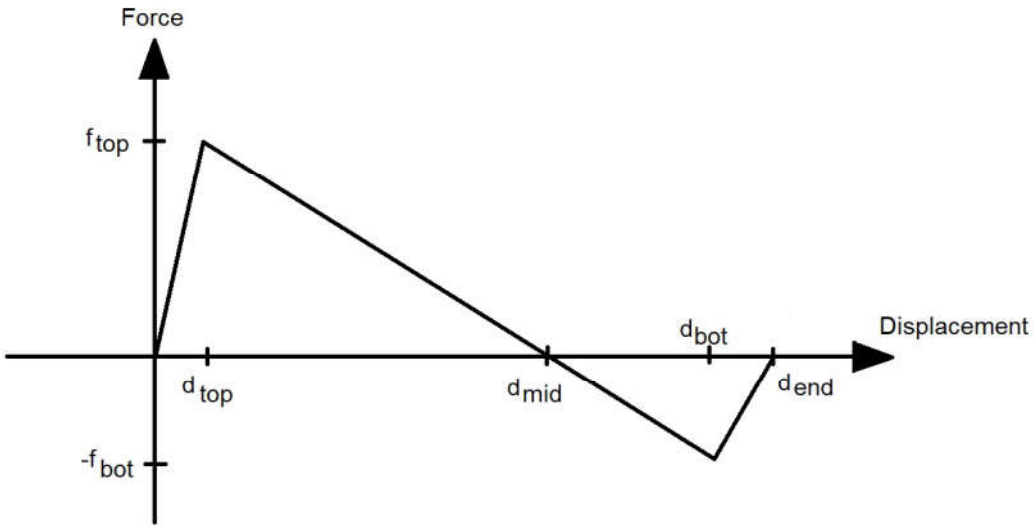


Figure 2.6. Force-displacement graph for a curved beam whose second buckling mode is constrained [52].

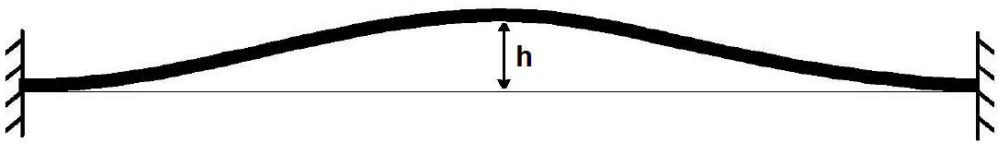


Figure 2.7. Apex height for the curved beam [52].

Force-displacement graph for the second-mode-constrained curved beam is shown in Figure 2.6. Apex height of the negative stiffness beam is shown in Figure 2.7.

The slope of the curve in the force-displacement graph gives the stiffness of the beam. The slope is negative between d_{top} and d_{bot} which means the stiffness of the beam is negative for the specified range.

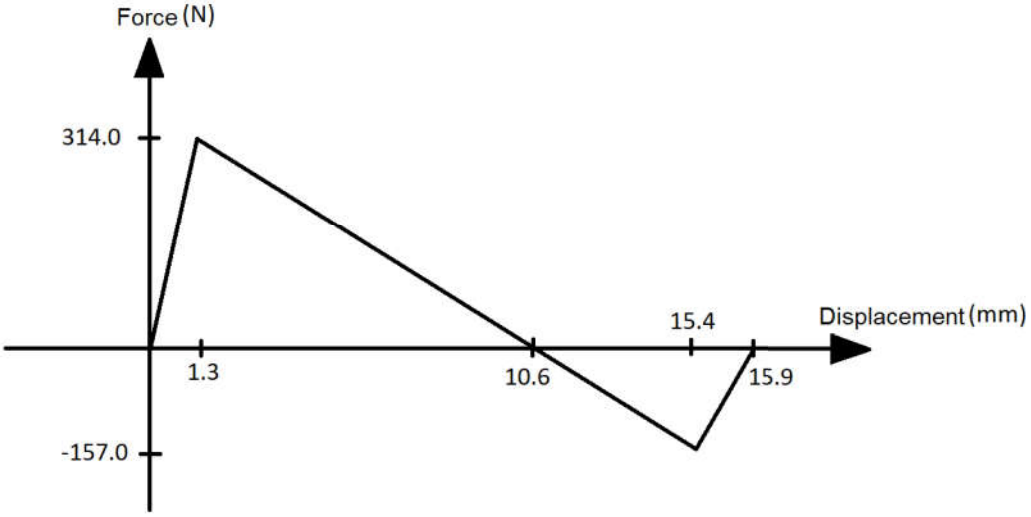


Figure 2.8. Force-displacement graph for the designed curved beam.

The peak force in the system should exceed 240 N and the negative stiffness region should provide at least 8 mm stroke. Hence, the parameters of the system are chosen as E_n=200 GPa, b_n=20 mm, t_n=0.8 mm, l_n= 186 mm, h= 8 mm. When these parameters are inserted into the graph shown in Figure 2.6, the graph in Figure 2.8 is obtained. There are two negative stiffness beams in the design. Therefore, the forces in the graph are multiplied by 2.

The slope of the curve is calculated as

$$k_{n(Anal)} = -\frac{(314.0 + 157.0)}{(15.4 - 1.3)} = -33.4 \text{ N/mm}. \tag{2.32}$$

Negative stiffness can also be found by using Equation 2.30 and Equation 2.31 as

$$k_{n(Anal)} = -2\frac{1110E_nI_n}{1.76l_n^3} = -33.4 \text{ N/mm}. \tag{2.33}$$

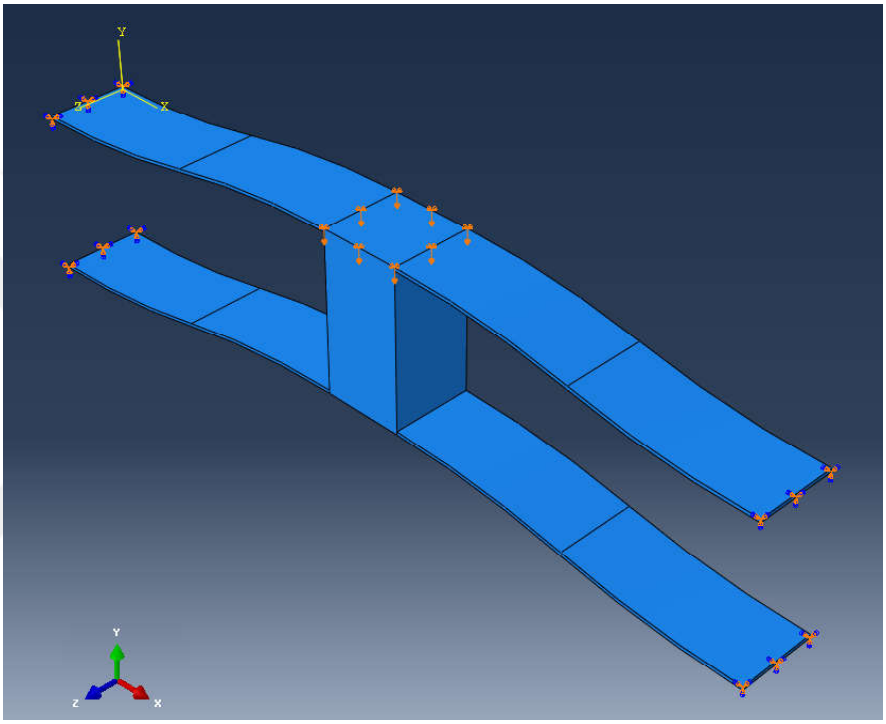


Figure 2.9. FEM model of the negative stiffness elements.

The negative stiffness elements are also modeled and analyzed by using Finite Element Method(FEM). Abaqus CAE software is used to get FEM solution. Clamped-clamped boundary conditions for the beams are provided and shown in Figure 2.9. Moreover, displacement is applied to the central part in 1000 increments and the reaction force is calculated for each increment. Large deflections are considered in the analysis. Consequently, force-displacement curve for the finite element analysis is obtained.

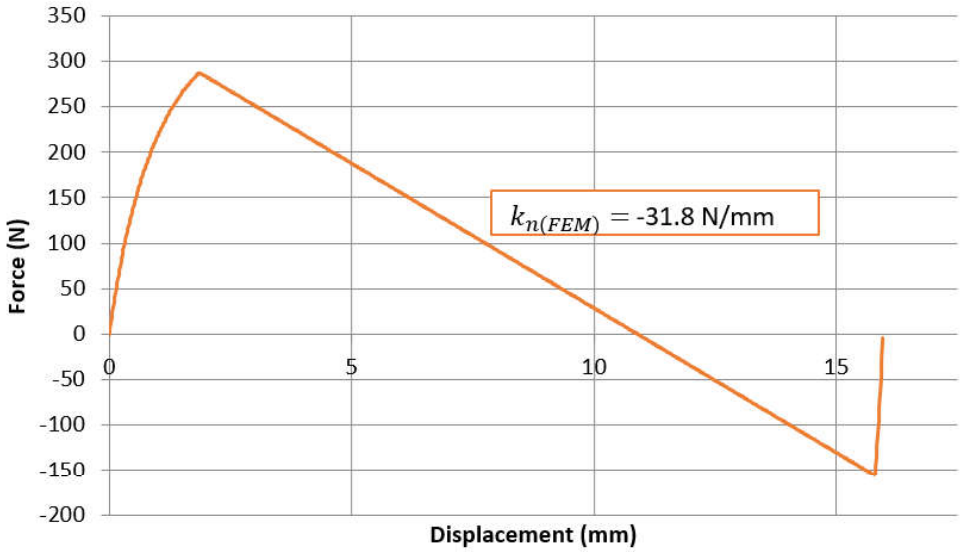


Figure 2.10. Force-displacement graph for the FEM model.

The negative stiffness value for the FEM solution can be found by calculating the slope of the middle part of the force-displacement curve as

$$k_{n(FEM)} = -\frac{(287.1 + 155.4)}{(15.8 - 1.8)} = -31.8 \text{ N/mm}. \tag{2.34}$$

2.1.2.2. Positive Stiffness Element. A helical compression spring with elliptical cross section is used as a positive stiffness element in the design. Helical springs with an elliptical cross-section have larger stroke than those with a circular cross-section for the same free height. As a result, the mounting height can be decreased [53].

The spring constant with elliptical cross-section can be calculated analytically in the same way as for the circular cross-section using Castigliano's theorem [53]:

$$k_{p(Anal)} = \frac{Ga^3b^3}{2n_a(a^2 + b^2)R^3}. \tag{2.35}$$

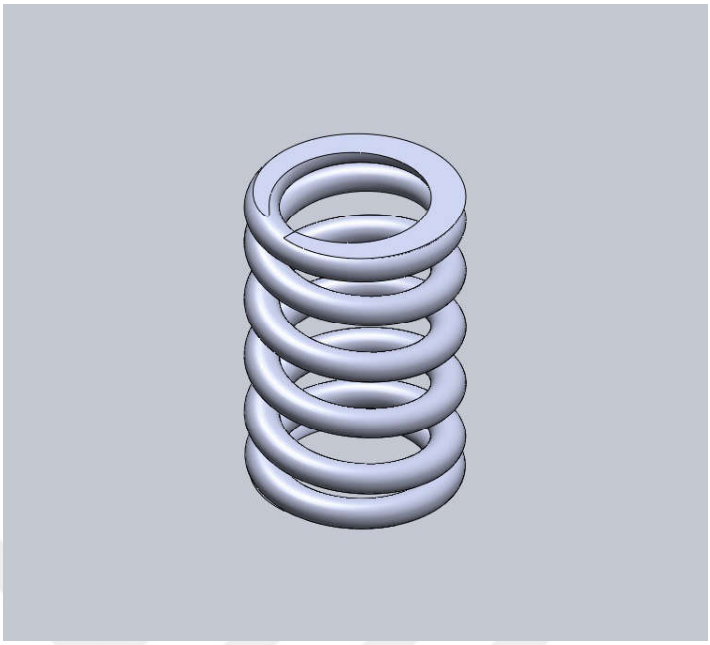


Figure 2.11. Helical compression spring with elliptical cross section.

Here, n_a is the active number of coils in the spring, G is the material shear modulus, a and b are half of the dimensions of elliptical cross-section, R is the mean coil radius. The type of the spring end affects the number of active coils. The spring that is used in the design has squared and ground end type. According to Wahl [54], the active number of coils are equivalent to a deduction of 2 turn from total number of coils. The aim is to achieve a positive stiffness value around 30 N/mm. Hence, the parameters of the spring are chosen as G= 80 GPa , $2a$= 3.35 mm , $2b$= 4.10 mm, n_a= 5 , R= 11.4 mm. When these parameters are inserted into Equation (2.35), the positive stiffness value for the spring is obtained as

$$k_{p(Anal)} = 31.2 \text{ N/mm}. \tag{2.36}$$

The helical compression spring is modeled in the finite element analysis software. One end of the helical spring is restricted to prevent the movement in the applied force direction and the other end of the spring is free to move.

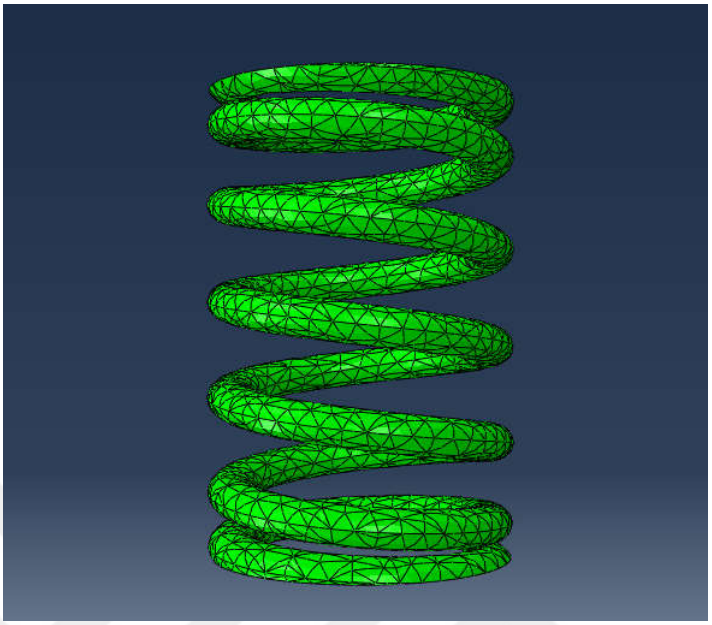


Figure 2.12. FEM model of the helical spring with elliptical cross section.

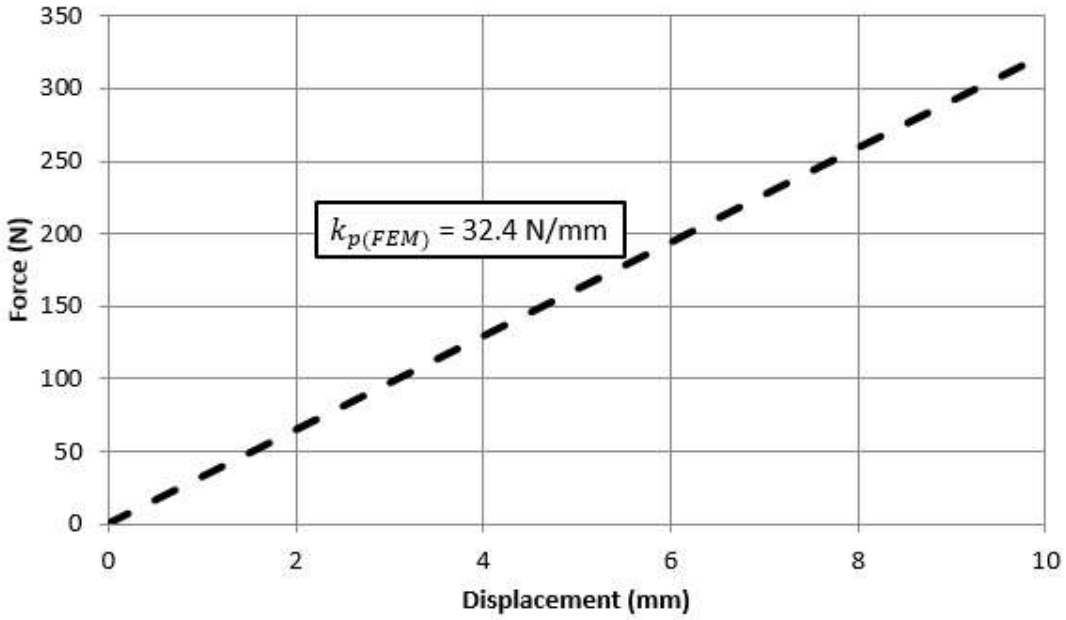


Figure 2.13. Force-displacement graph for FEM solution of the helical compression spring with elliptical cross section.

From the free end, a force is applied to the spring and force-displacement curve is obtained. As shown in Figure 2.13, the stiffness is calculated from the slope of the curve as

$$k_{p(FEM)} = 32.4 \text{ N/mm}. \tag{2.37}$$

Notice that the analytical and finite element results for the positive stiffness value are close (compare Equation (2.36) and Equation (2.37)). So, these two models are compatible.

The wire at the center also works as a positive stiffness element in the system. The axial stiffness of the wire can be calculated as

$$k_{w(Anal)} = \frac{E_w A_w}{l_{wf}} \tag{2.38}$$

and the cross sectional area of the wire can be calculated as

$$A_w = \pi r_w^2 \tag{2.39}$$

where E_w is the elastic modulus of the wire, A_w is the cross sectional area of the wire, l_{wf} is the full length of the wire and r_w is the radius of the wire. Axial stiffness of the wire is calculated by inserting the wire parameters (E_w= 210 GPa , r_w= 0.5 mm, l_{wf}= 235 mm) into Equation (2.38) and Equation (2.39). Consequently, axial stiffness value for the wire is obtained as

$$k_{w(Anal)} = 701.8 \text{ N/mm}. \tag{2.40}$$

The positive stiffness elements which are helical compression spring with elliptical cross section and the wire are connected in series. The equivalent positive stiffness can be calculated as

$$k_{pt(Anal)} = \left(\frac{1}{k_{p(Anal)}} + \frac{1}{k_{w(Anal)}} \right)^{-1}. \tag{2.41}$$

When $k_{p(Anal)}$ and $k_{w(Anal)}$ in Equation (2.36) and Equation (2.40) are inserted into Equation (2.41), $k_{pt(Anal)}$ can be found as

$$k_{pt(Anal)} = 29.9 \text{ N/mm}. \tag{2.42}$$

2.1.3. Complete Design

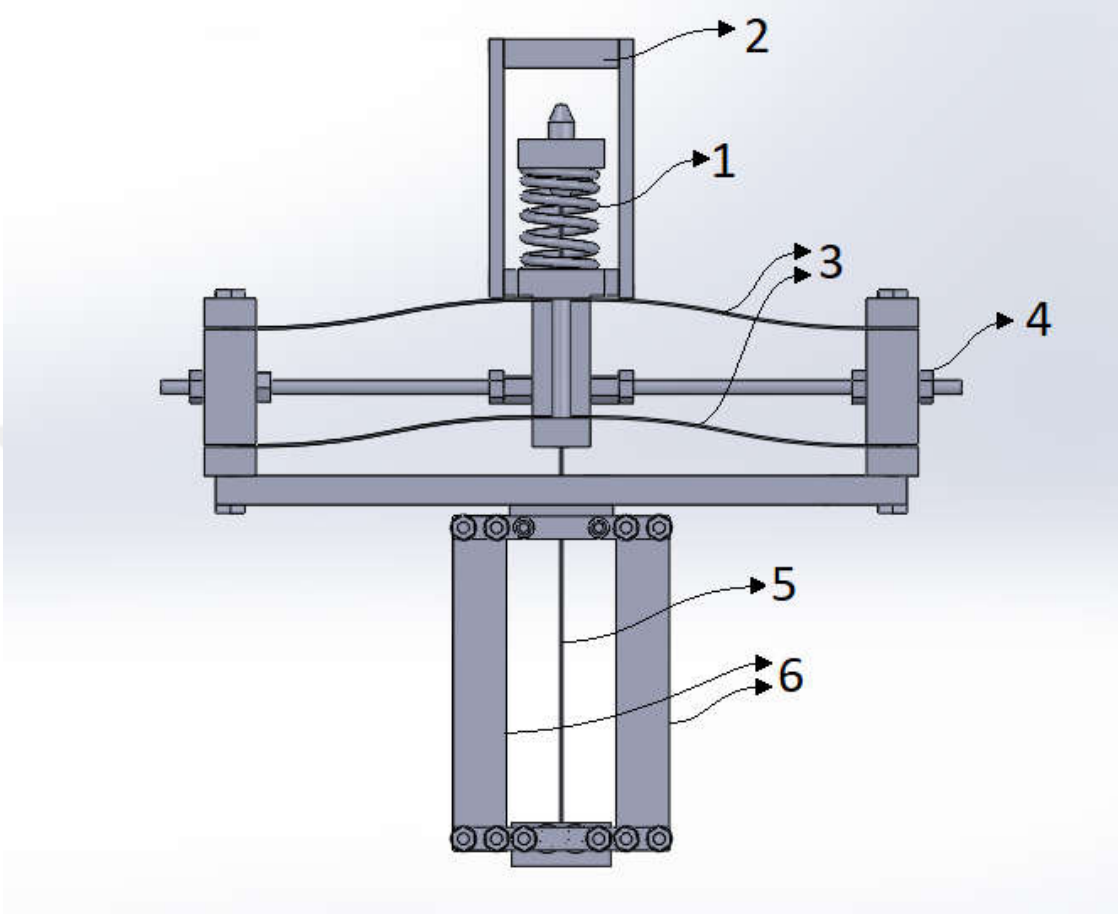


Figure 2.14. Front view of adjustable stiffness vibration isolator/absorber system: 1 - Helical spring, 2 - Spring cover plate, 3 - Negative stiffness beams, 4 - Adjustment nut, 5 - Tension wire, 6 - Parallel beam set

The system has two main parts and these two parts are connected to each other with a wire. Front view of the system with some marked key elements is shown in Figure 2.14. The helical spring, spring cover plate, negative stiffness beams, adjustment nut, the wire and parallel beam set are marked with 1, 2, 3, 4, 5 and 6 respectively. The adjustment nut (4) is used to adjust the apex height (h) of the negative stiffness beams (3). Once the desired apex height is obtained, the spring cover plate (2) can be moved to adjust the tension in the wire (5). Tension in the wire changes as the helical spring (1) is compressed. Since the negative stiffness of the beams (3) is almost equal to the positive stiffness of the helical spring (1), tension in the wire can be changed with almost zero effort. Wire tension force also compresses the parallel beam set (6).

As a result, the stiffness of the free end of the parallel beam set (6) can be adjusted by just moving the spring cover plate (2). Due to stiffness adjustment, natural frequency of the tip of the parallel beam set changes.

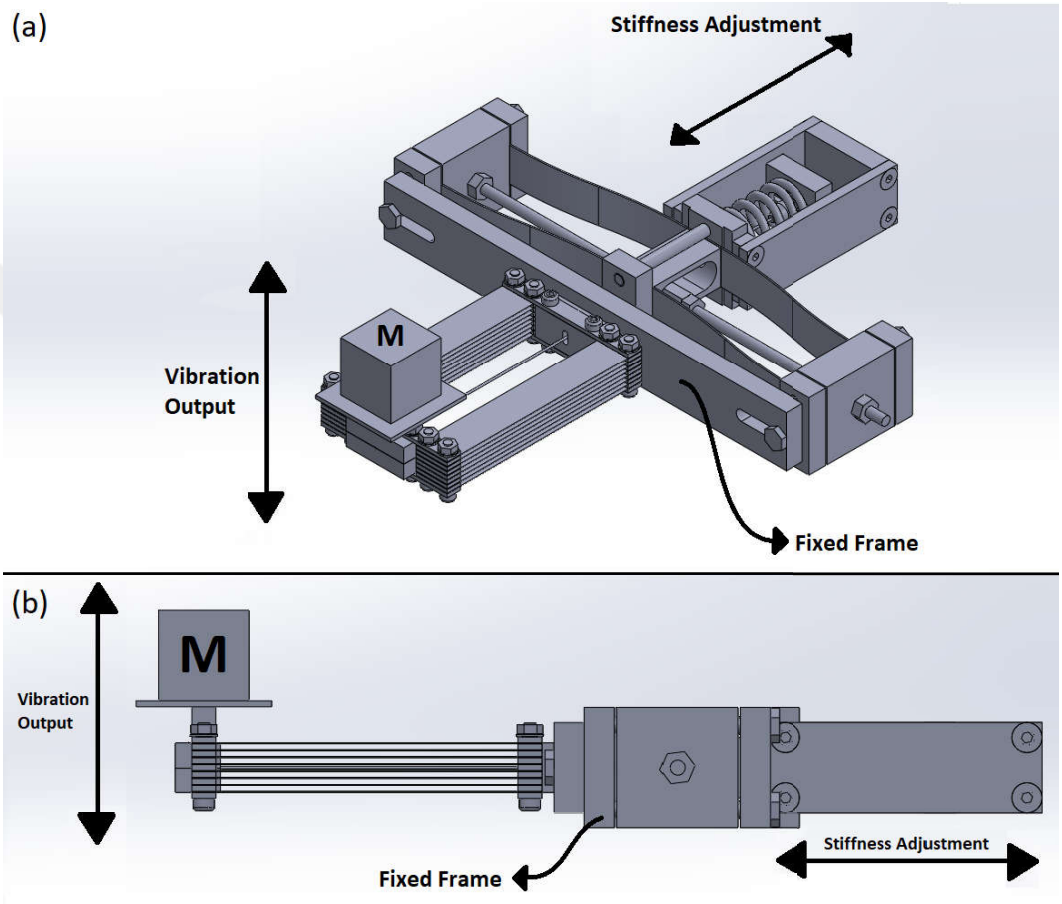


Figure 2.15. (a) Isometric view of the adjustable stiffness vibration isolator/ absorber system. (b) Side view of the adjustable stiffness vibration isolator/absorber system.

Positive stiffness and negative stiffness systems work in parallel configuration. The stiffness of the system approaches zero since the positive and negative stiffness values are close to each other. With almost zero stiffness, the helical spring can be compressed up to 8.5 mm. The equivalent positive stiffness is approximately 29.9 N/mm. A reaction force of around 240 N occurs after 8 mm of compression. This force is transmitted to the parallel beam set via the wire. Since the critical buckling force of the parallel beam set is 243.2 N according to Equation (2.22), the parallel beam set approaches buckling and the stiffness goes to zero when the apex height of

the quasi-zero stiffness mechanism is equal to 8.13 mm. The natural frequency drops to zero when the critical buckling force is approached (P=-P_{cr}) according to Equation (2.10). By using Equation (2.10), the first transverse natural frequency of the axially loaded beams is calculated and tabulated in Table 2.1 for every 1 mm of compression of the quasi-zero stiffness mechanism. The compression force decreases by 29.9 N per 1 mm of compression of quasi-zero stiffness mechanism. The first transverse natural frequency of axially loaded beams without axial load is obtained by Equation (2.9).

Table 2.1. The first transverse natural frequency of the system for different compression values in mm.

	Natural Frequency
0 mm	0 Hz
1 mm	5.853 Hz
2 mm	8.269 Hz
3 mm	10.124 Hz
4 mm	11.689 Hz
5 mm	13.067 Hz
6 mm	14.313 Hz
7 mm	15.459 Hz
8 mm	16.526 Hz
8.13 mm	16.660 Hz

The overall stiffness of the complete system can be found by using Equation (2.33) and Equation (2.41) as

$$k = k_{n(Anal)} + k_{pt(Anal)}. \tag{2.43}$$

For the current parameters of the system, the negative stiffness is around -30 N/mm and the positive stiffness is around 30 N/mm resulting in near zero stiffness while adjusting the tension in the wire. As a result, axial load on the parallel beam set can be adjusted with almost zero effort.

3. EXPERIMENTAL RESULTS AND DISCUSSION

In this section of the thesis, testing of the vibration isolation system is covered. A universal testing machine (Zwick-Roell Z010), a laser vibrometer (Polytec PDV 100), a data acquisition device (Polytec VIB-E-220) and a computer is used to conduct the experiments. Force-displacement analyses for negative stiffness element, quasi-zero stiffness system and helical spring have been performed by using the universal testing machine. Additionally, natural frequency of the system is measured with the laser vibrometer for different wire tension values.

In the first experiment, negative stiffness element of quasi-zero stiffness mechanism is compressed with the universal testing machine. Helical spring is removed from the system for the first experiment. Force-displacement curve of the negative stiffness element of quasi-zero stiffness mechanism is obtained. Linear regression analysis has been done for the curve where the slope is negative. The maximum compression force is equal to 262.4 N. Moreover, slope of the line gives the negative stiffness value created by the negative stiffness element and it is equal to

$$k_{n(exp)} = -30.3 \text{ N/mm}. \tag{3.1}$$

In the second experiment, helical spring is added to the system and compression test is repeated. Force-displacement graph of quasi-zero stiffness mechanism is acquired. The maximum force did not exceed 10 N. This will enable that natural frequency of the system can be changed with very small effort compared to the actual effort to compress the beams, which is more than 250 N.

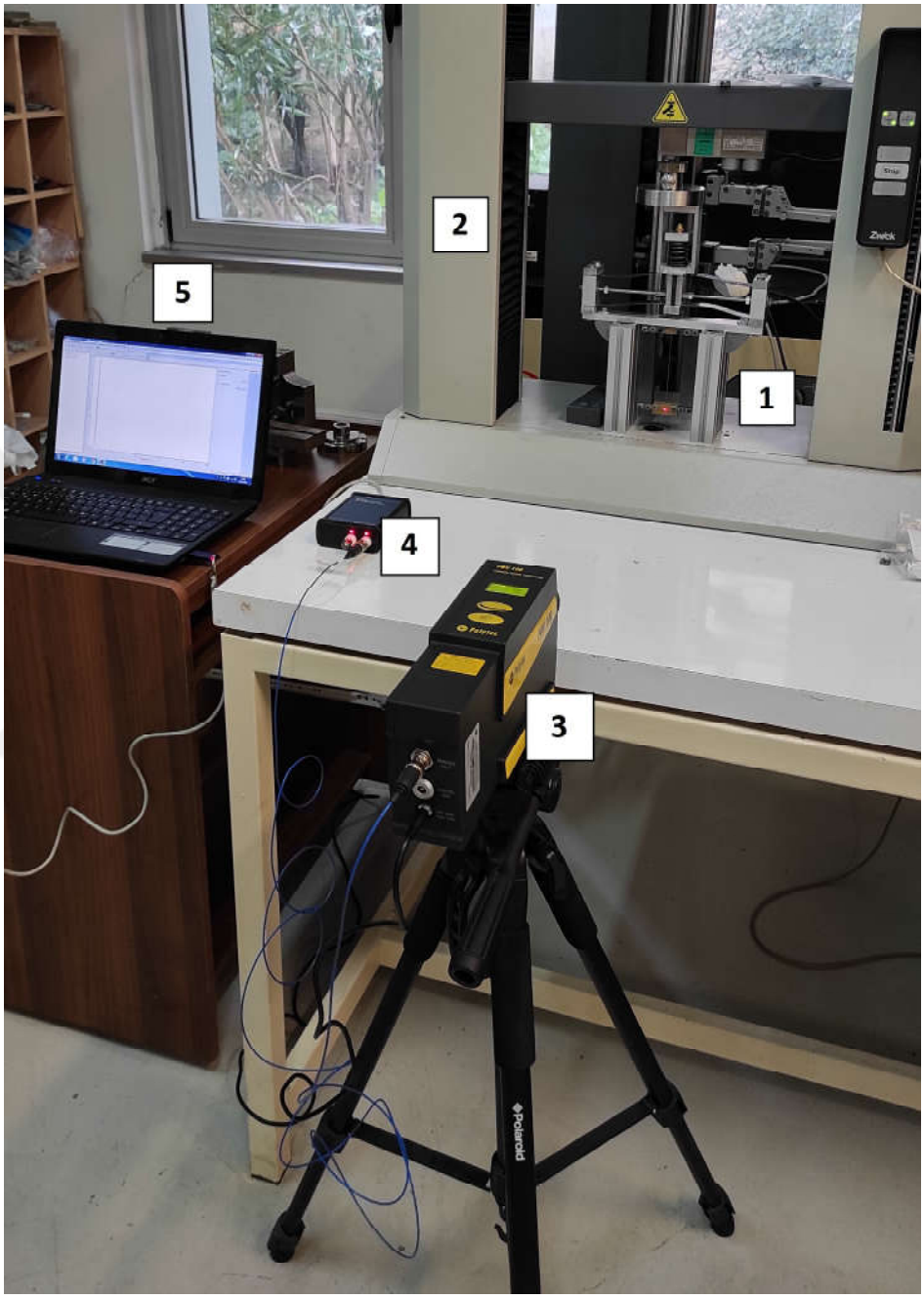


Figure 3.1. The experimental setup showing the prototype (1) that is compressed by the universal testing machine (2), meanwhile the laser vibrometer (3) measures the vibration velocity of the block at the free end of the parallel beam set. The vibration data is obtained through the data acquisition system (4) and the data is analyzed by the computer (5).

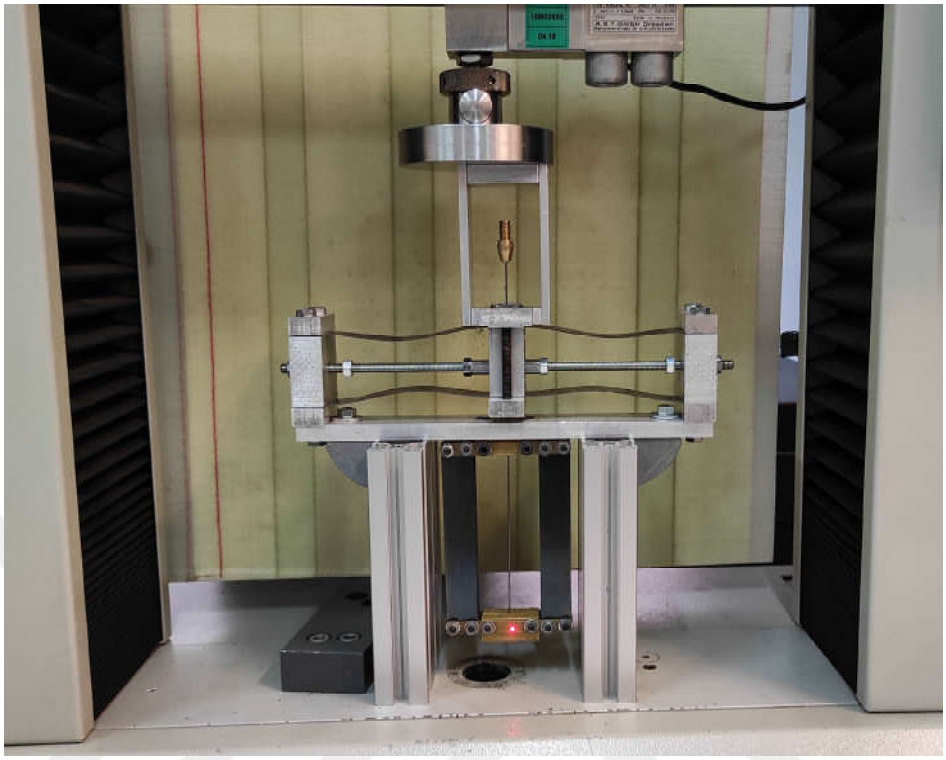


Figure 3.2. Compression test of negative stiffness element.

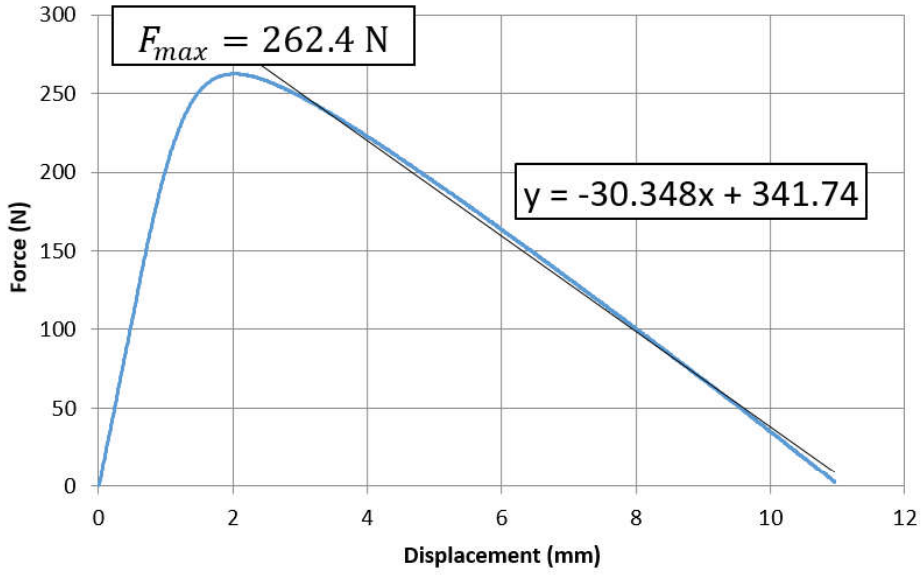


Figure 3.3. Experimental force-displacement graph of the negative stiffness element.

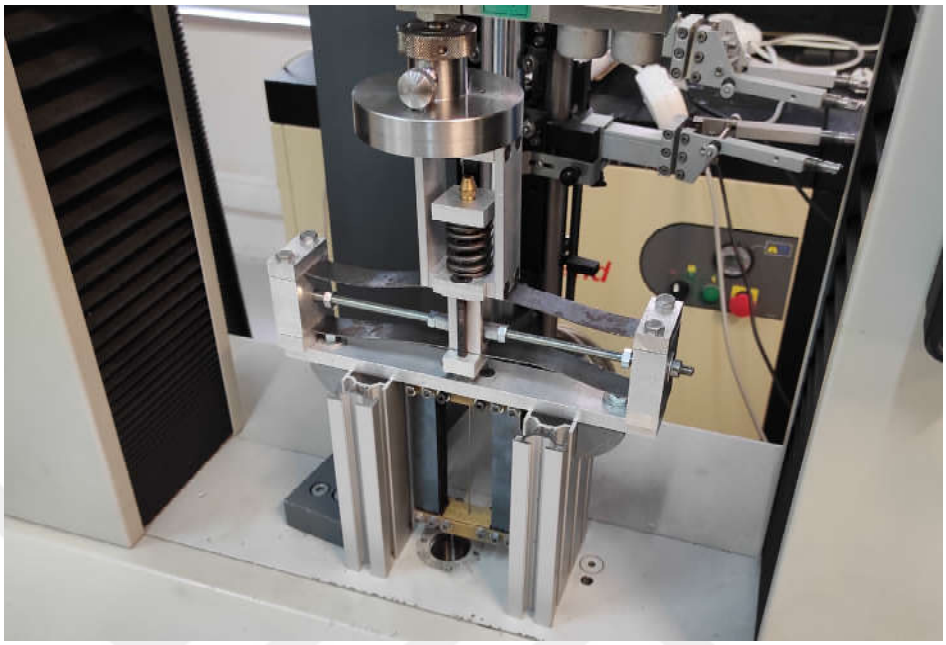


Figure 3.4. Compression test of quasi-zero siffness system.

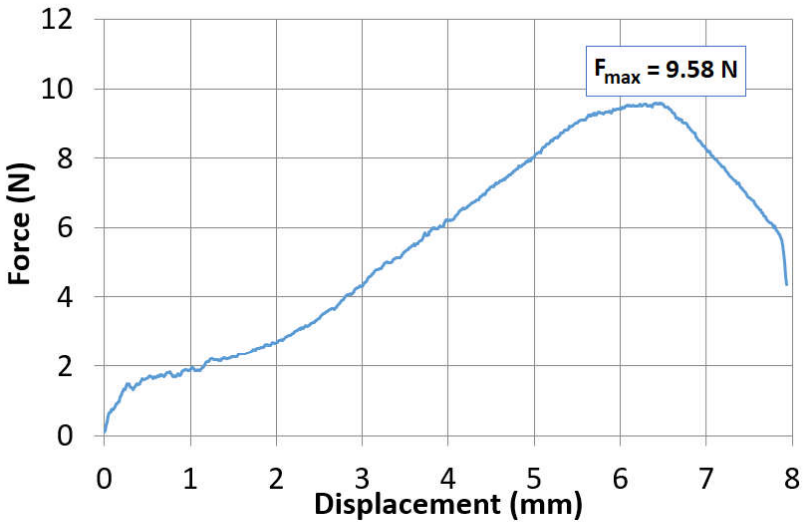


Figure 3.5. Experimental force-displacement graph of the quasi-zero stiffness system.

In the third experiment, compression test is repeated with the maximum speed of the universal testing machine which is equal to 16 mm/s. The spring cover plate is compressed by 8 mm in 0.5 seconds. The system is returned to its initial position after 2.5 seconds of pause. Vibration velocity of the block at the free end of the parallel beam set is measured by the laser vibrometer.

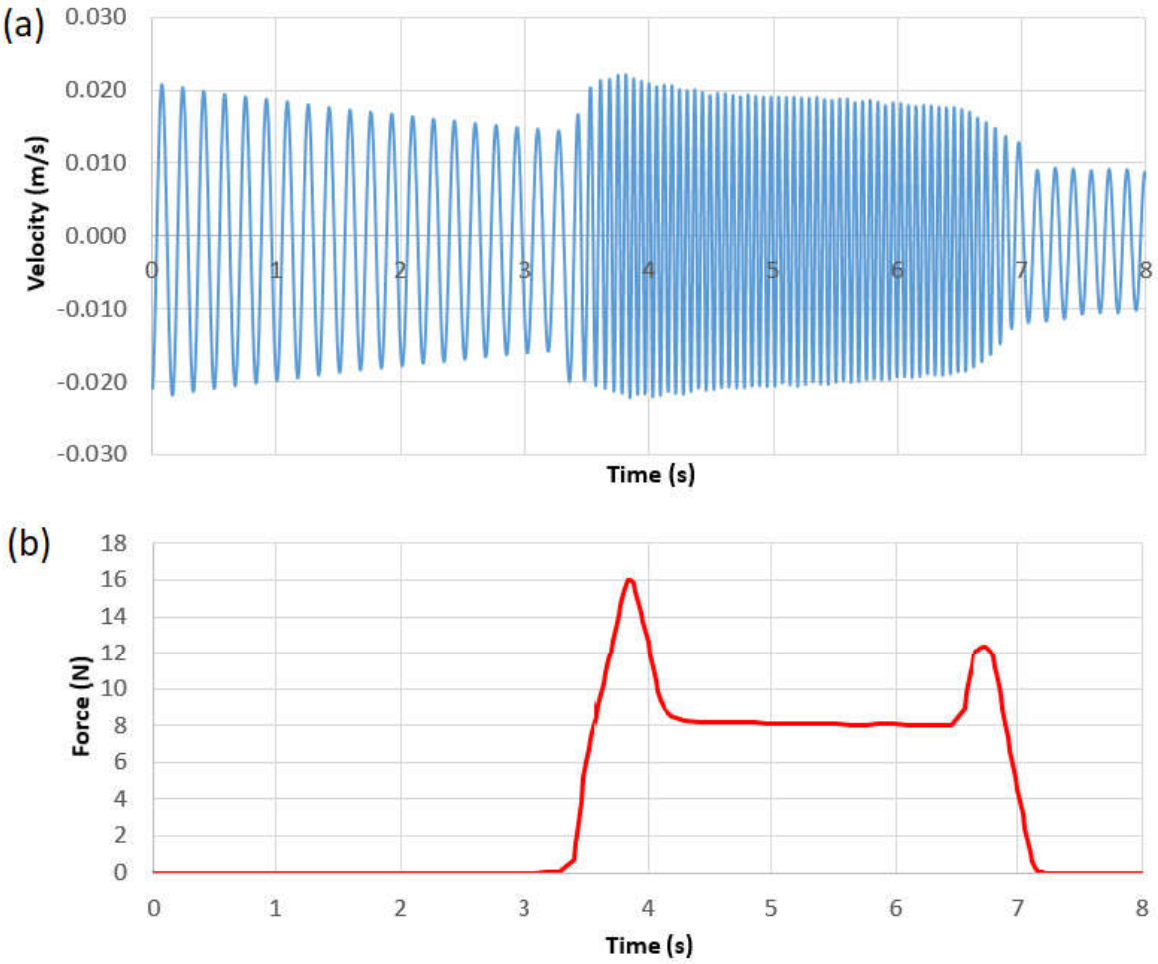


Figure 3.6. (a) Experimental velocity-time graph of the block at the free end of the parallel beam set in the quasi-zero stiffness system. (b) The corresponding force-time graph that is required to adjust the system.

Velocity versus time graph is shown in Figure 3.6(a). In Figure 3.6(b), force response of the mechanism is shown for the corresponding time period. Although the system was compressed quickly, the maximum force did not exceed 16 N. This experi-

ment demonstrated that the natural frequency of the system can be changed with very small effort and also the response time of the system is very short.

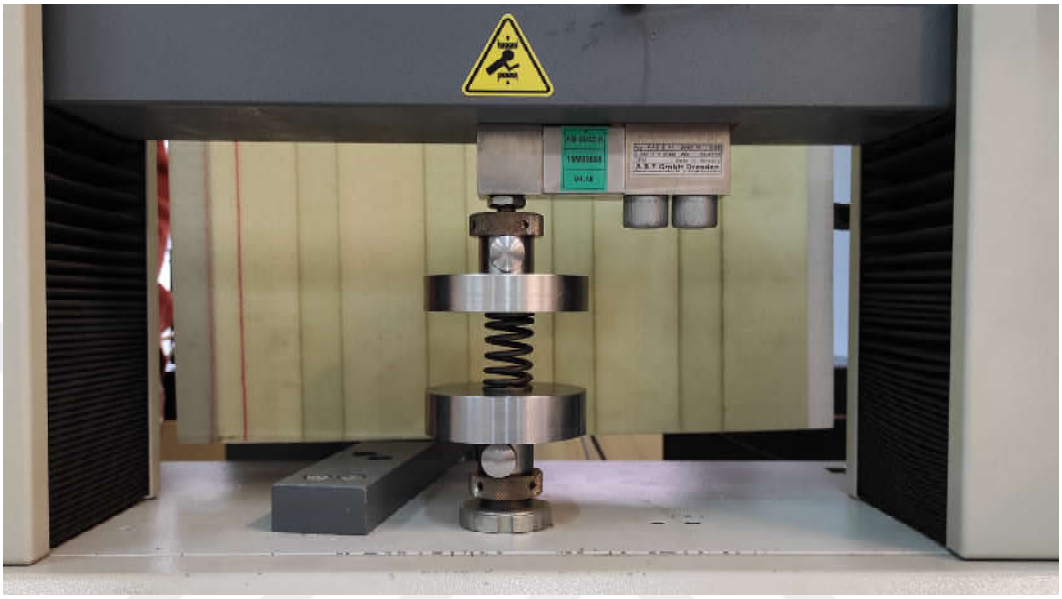


Figure 3.7. Compression test of helical spring.

In the fourth experiment, compression test of the helical spring has been carried out as can be seen in Figure 3.7. Force-displacement graph of helical spring is obtained. Slope of the line can be calculated by linear regression analysis, which gives the positive stiffness of the helical spring as

$$k_{p(exp)} = 29.8 \text{ N/mm}. \tag{3.2}$$

In the last experiment, natural frequency of the system is measured with the help of a laser vibrometer. Initially, the helical spring is fully compressed by extending the spring cover plate upwards. When the cover plate is compressed, the compression in the helical spring decreases, which in turn reduces the tension in the wire and the natural frequency increases. At every 1 mm of compression, oscillation frequency is measured from the tip of the free end of axially loaded parallel beam set.

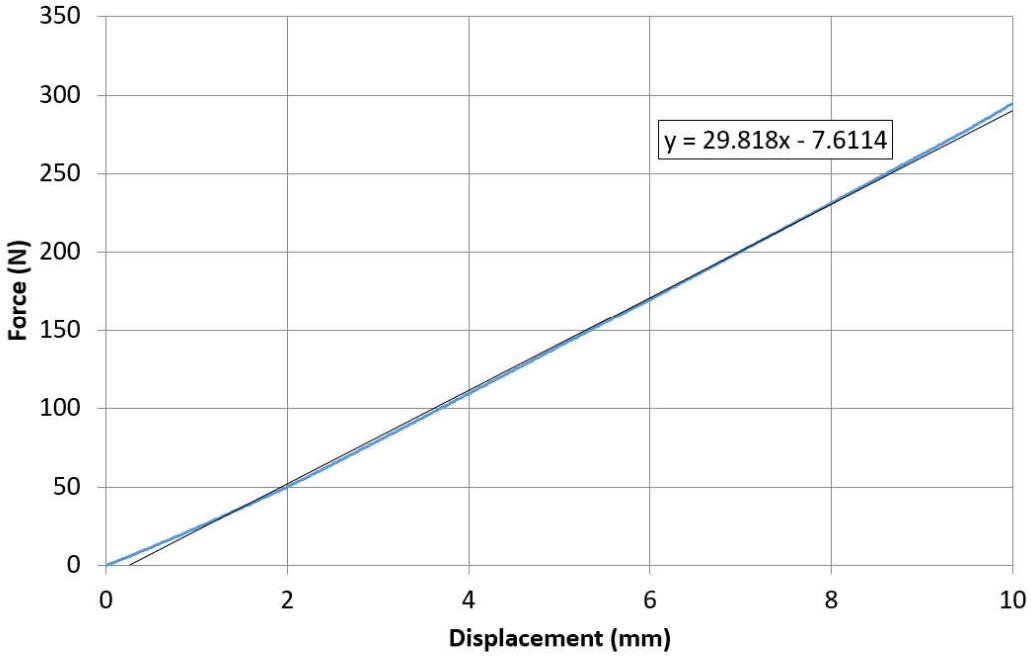


Figure 3.8. Experimental force-displacement graph of the helical spring.

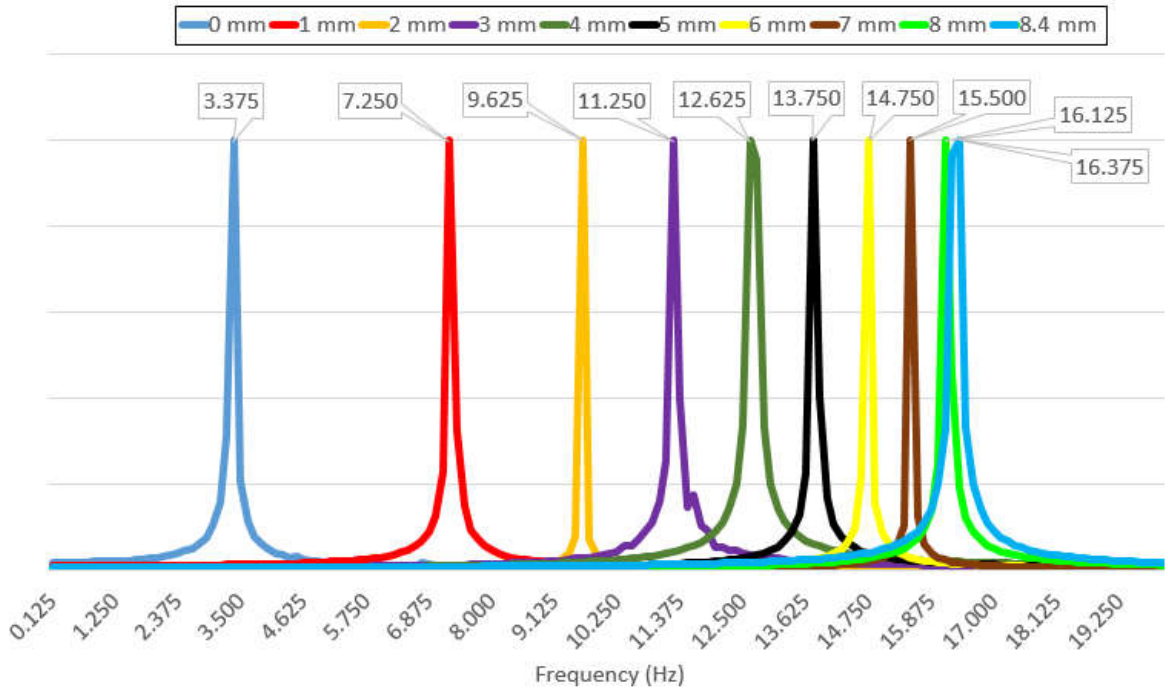


Figure 3.9. Natural frequency of the system for different compression values.

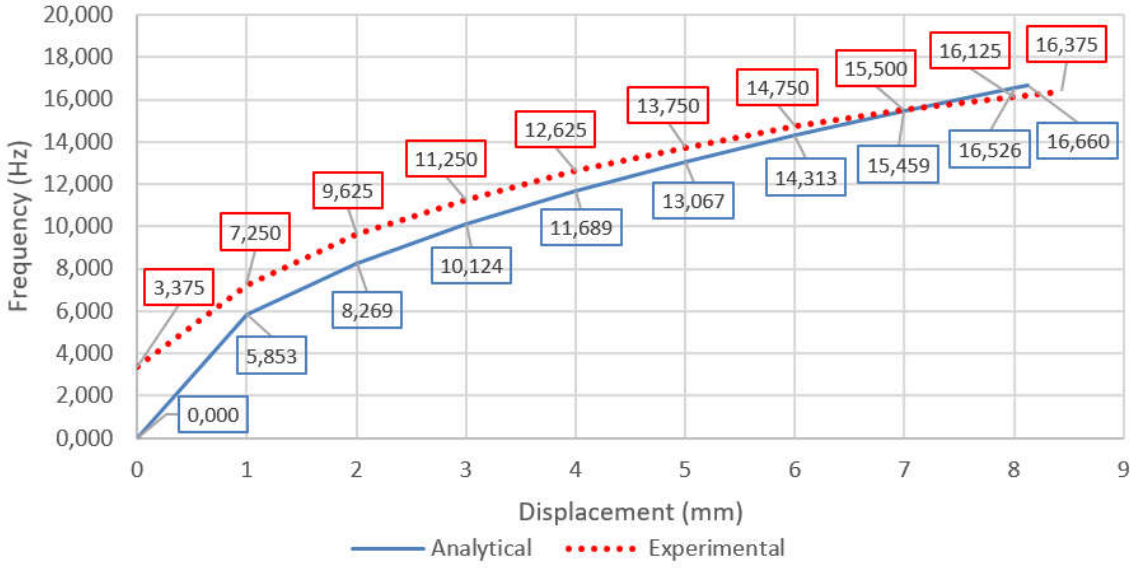


Figure 3.10. Analytical and experimental results for natural frequency.

In Figure 3.9 frequency responses of the system for the corresponding compression distances are shown and in Figure 3.10 measured natural frequencies of adjustable stiffness vibration isolation system are compared with the analytical results.

In Section 2, analytical model and finite element model of the adjustable stiffness vibration isolation system was introduced. After production of the system, experiments have been conducted. In this section, analytical, finite element and experimental results for the helical spring which is used as the positive stiffness element in the system will be compared. The experimental results of positive stiffness is smaller than the results found from the analytical study and FEM. The errors for the positive stiffness are 4.5% for analytical study and 8.0% for FEM.

The experimental results of negative stiffness is higher than the results found from the analytical study and FEM. The errors for the negative stiffness are 9.3% for analytical study and 4.7% for FEM.

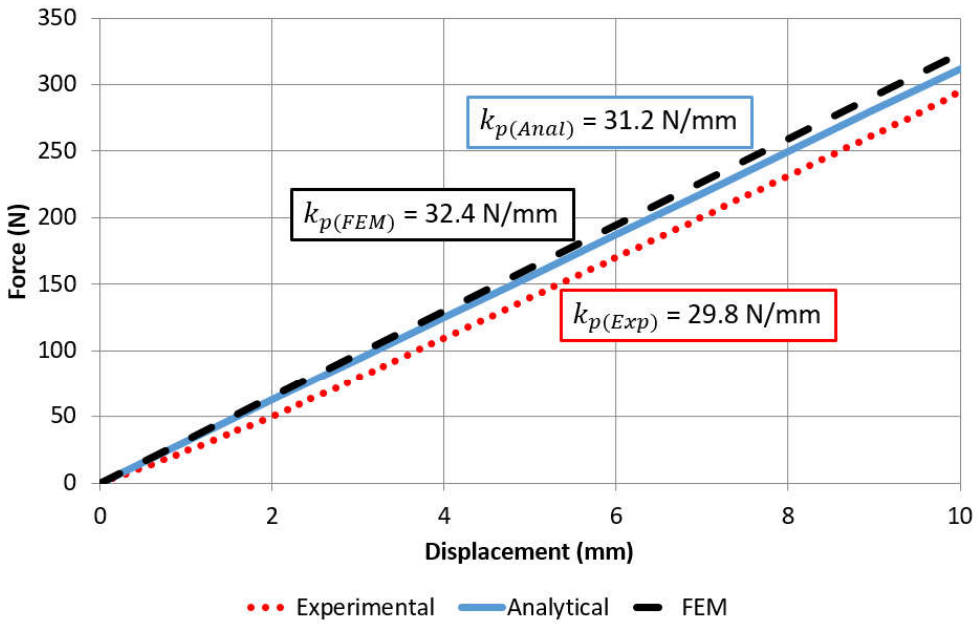


Figure 3.11. Analytical, finite element and experimental results for the helical spring.

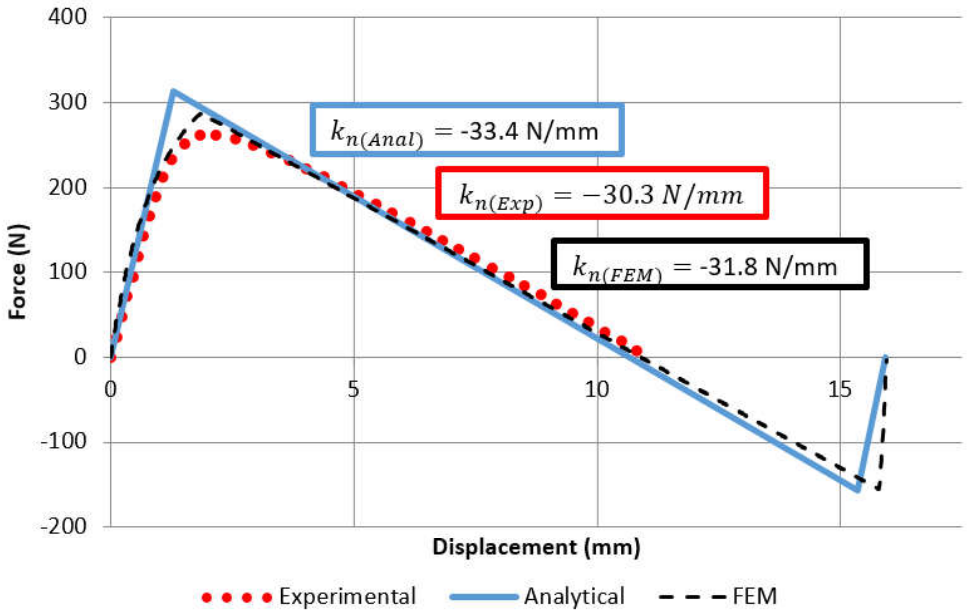


Figure 3.12. Analytical, finite element and experimental results for negative stiffness element.

Notice that the peak force values in Figure 3.12 are different. Especially, the experimental peak force value is lower. Due to manufacturing inaccuracies, the negative stiffness beams do not symmetrically buckle. Moreover, the frame that is used to hold these beams is not perfectly rigid. These factors reduce the peak force in the graph. Nevertheless, the slopes of the curves in the negative stiffness region are close to each other. Consequently, the total stiffness of the experimental setup is close to zero and the effort to control the natural frequency of the system is very low. In order to change the natural frequency of the system from 3.4 Hz to 16.4 Hz, the spring cover plate should be compressed by 8.4 mm. Since, the effort is less than 10 N in the displacement range, stiffness change can be made very easily. If the stiffness is changed very quickly as in Figure 3.6, the required force can increase to 16 N. However, without the negative stiffness subsystem, more than 250 N would be required to change the natural frequency in the same range.

4. CONCLUSION

In this thesis, a new vibration isolator/absorber system with adjustable stiffness is provided. The system has two main parts; axially loaded beams and quasi-zero stiffness mechanism. A wire is used to transmit the axial force to the beams, which is connected to the free ends of the axially loaded beams and the quasi-zero stiffness mechanism. Quasi-zero stiffness mechanism, which is composed of a negative stiffness element and a positive stiffness element, is used to decrease the force that is needed to change the stiffness of the system. To have a compact system, positive stiffness element is chosen as an elliptical cross section helical spring. Moreover, the negative stiffness element is composed of buckled beams whose length can be selected so that the negative stiffness can match the positive stiffness in the system. Both analytical and finite element model of the system are analyzed. Then the system is manufactured and tested. Experimental results are compared with the results of analytical and finite element models and it is shown that the stiffness results are close to each other.

The manufactured prototype shows that the stiffness of the system can be adjusted with very small effort. Moreover, response time of the system is very short. Natural frequency of the system can be adjusted between 3.4 Hz and 16.4 Hz with almost zero effort with the help of the quasi-zero stiffness mechanism. It is possible to bring the lower frequency limit of the system closer to zero, but in that case stability problems can arise. Therefore, the lower frequency limit was not lowered further. The stiffness of the system can be changed more than 20 times.

REFERENCES

1. Singiresu, S. R., *Mechanical Vibrations*, Addison Wesley, 1995.

2. Bishop, R. E. D. and D. C. Johnson, *The Mechanics of Vibration*, Cambridge University Press, 2011.

3. Tantanawat, T., Z. Li and S. Kota, "Application of Compliant Mechanisms to Active Vibration Isolation Systems", *ASME 2004 International Design Engineering Technical Conferences and Computers and Information in Engineering Conference*, pp. 1165–1172, American Society of Mechanical Engineers Digital Collection, 2004.

4. Smith, M. C. and F.-C. Wang, "Performance Benefits In Passive Vehicle Suspensions Employing Inerters", *Vehicle System Dynamics*, Vol. 42, No. 4, pp. 235–257, 2004.

5. Prawoto, Y., M. Ikeda, S. Manville and A. Nishikawa, "Design and Failure Modes of Automotive Suspension Springs", *Engineering Failure Analysis*, Vol. 15, No. 8, pp. 1155–1174, 2008.

6. Gowd, G. H. and E. V. Goud, "Static Analysis of Leaf Spring", *International Journal of Engineering Science and Technology*, Vol. 4, No. 8, pp. 3794–3803, 2012.

7. Tajima, J., F. Momiyama and N. Yuhara, "A New Solution for Two-Bag Air Suspension System with Leaf Spring for Heavy-Duty Vehicle", *Vehicle System Dynamics*, Vol. 44, No. 2, pp. 107–138, 2006.

8. Balaji, P., M. Rahman, L. Moussa and H. H. Lau, "Wire Rope Isolators for Vibration Isolation of Equipment and Structures–A Review", *IOP Conference Series: Materials Science and Engineering*, Vol. 78, p. 012001, IOP Publishing, 2015.

9. Ni, Y., J. Ko, C. Wong and S. Zhan, "Modelling and Identification of a Wire-Cable Vibration Isolator via a Cyclic Loading Test", *Proceedings of the Institution of Mechanical Engineers, Part I: Journal of Systems and Control Engineering*, Vol. 213, No. 3, pp. 163–172, 1999.

10. Chungui, Z., Z. Xinong, X. Shilin, Z. Tong and Z. Changchun, "Hybrid Modeling of Wire Cable Vibration Isolation System Through Neural Network", *Mathematics and Computers in Simulation*, Vol. 79, No. 10, pp. 3160–3173, 2009.

11. Mallik, A., V. Kher, M. Puri and H. Hatwal, "On The Modelling of Non-Linear Elastomeric Vibration Isolators", *Journal of Sound and Vibration*, Vol. 219, No. 2, pp. 239–253, 1999.

12. Sjoberg, M. M. and L. Kari, "Non-Linear Behavior of a Rubber Isolator System Using Fractional Derivatives", *Vehicle System Dynamics*, Vol. 37, No. 3, pp. 217–236, 2002.

13. Genovese, A., S. Strano and M. Terzo, "Model-Based Study of a Resonant System in a Railway Air Spring Secondary Suspension for Energy Harvesting Applications", *Proceedings of the 2018 2nd International Conference on Mechatronics Systems and Control Engineering*, pp. 45–51, 2018.

14. Zhang, J., S. Chen, Z. Wu, L. Yang and B. Zhang, "Research on Nonlinear Characteristics of Hydro-Pneumatic Spring and Impact to Ride Performance of Vehicles", *Proceedings of the FISITA 2012 World Automotive Congress*, pp. 1211–1222, Springer, 2013.

15. Gavriloski, V., J. Jovanova, G. Tasevski and M. Didrov, "Development of a New Air Spring Dynamic Model", *FME Transactions*, Vol. 42, No. 4, pp. 305–310, 2014.

16. Anh, N., H. Matsuhisa, L. Viet and M. Yasuda, "Vibration Control of an Inverted Pendulum Type Structure by Passive Mass–Spring-Pendulum Dynamic Vibration

Absorber", *Journal of Sound and Vibration*, Vol. 307, No. 1-2, pp. 187–201, 2007.

17. Hunt, J. B. and J.-C. Nissen, "The Broadband Dynamic Vibration Absorber", *Journal of Sound Vibration*, Vol. 83, No. 4, pp. 573–578, 1982.

18. Jiang, S. L., T. J. Yang, J. T. Du and Y. Y. Hu, "Research on Frequency-Tuned Dynamic Vibration Absorber", *Applied Mechanics and Materials*, Vol. 66, pp. 1762–1768, Trans Tech Publ, 2011.

19. Nguyen, D. C., "Vibration Control of a Rotating Shaft by Passive Mass-Spring-Disc Dynamic Vibration Absorber", *Archive of Mechanical Engineering*, Vol. 67, 2020.

20. Barredo, E., J. M. Larios, J. Colín, J. Mayén, A. Flores-Hernández and M. Arias-Montiel, "A Novel High-Performance Passive Non-Traditional Inerter-Based Dynamic Vibration Absorber", *Journal of Sound and Vibration*, Vol. 485, p. 115583, 2020.

21. Hua, Y., W. Wong and L. Cheng, "Optimal Design of a Beam-Based Dynamic Vibration Absorber Using Fixed-Points Theory", *Journal of Sound and Vibration*, Vol. 421, pp. 111–131, 2018.

22. Sun, J., M. Jolly, and M. t. Norris, "Passive, Adaptive and Active Tuned Vibration Absorbers—A Survey", *Journal of Mechanical Design*, Vol. 117(B), pp. 234–242, 1995.

23. Alabuzhev, P., A. Gritchin, L. Kim, G. Migirenko, V. Chon and P. Stepanov, *Vibration Protection and Measuring Systems with Quasi-Zero Stiffness*, CRC Press, 1989.

24. Carrella, A., M. Brennan and T. Waters, "Static Analysis of a Passive Vibration Isolator with Quasi-Zero-Stiffness Characteristic", *Journal of Sound and Vibration*, Vol. 301, No. 3-5, pp. 678–689, 2007.

25. Huang, X., X. Liu, J. Sun, Z. Zhang and H. Hua, "Vibration Isolation Characteristics of a Nonlinear Isolator Using Euler Buckled Beam as Negative Stiffness Corrector: A Theoretical and Experimental Study", *Journal of Sound and Vibration*, Vol. 333, No. 4, pp. 1132–1148, 2014.

26. Den Hartog, J. P., *Mechanical Vibrations*, Courier Corporation, 1985.

27. Korenev, B. G. and L. M. Reznikov, *Dynamic Vibration Absorbers: Theory and Technical Applications*, John Wiley & Sons, 1993.

28. Acar, M. and C. Yilmaz, "Design of an Adaptive–Passive Dynamic Vibration Absorber Composed of a String–Mass System Equipped with Negative Stiffness Tension Adjusting Mechanism", *Journal of Sound and Vibration*, Vol. 332, No. 2, pp. 231–245, 2013.

29. Jalili, N., "A Comparative Study and Analysis of Semi-Active Vibration-Control Systems", *Journal of Vibration and Acoustics*, Vol. 124, No. 4, pp. 593–605, 2002.

30. Franchek, M., M. Ryan and R. Bernhard, "Adaptive Passive Vibration Control", *Journal of Sound and Vibration*, Vol. 189, No. 5, pp. 565–585, 1996.

31. Ghorbani-Tanha, A., M. Rahimian and A. Noorzad, "A Novel Semiactive Variable Stiffness Device and Its Application in a New Semiactive Tuned Vibration Absorber", *Journal of Engineering Mechanics*, Vol. 137, No. 6, pp. 390–399, 2011.

32. Nagarajaiah, S. and S. Sahasrabudhe, "Seismic Response Control of Smart Sliding Isolated Buildings Using Variable Stiffness Systems: An Experimental and Numerical Study", *Earthquake Engineering & Structural Dynamics*, Vol. 35, No. 2, pp. 177–197, 2006.

33. Jafari, A., N. G. Tsagarakis, B. Vanderborght and D. G. Caldwell, "A Novel Actuator with Adjustable Stiffness (AwAS)", *2010 IEEE/RSJ International Conference on Intelligent Robots and Systems*, pp. 4201–4206, 2010.

34. Cronje, J. M., P. S. Heyns, N. J. Theron and P. W. Loveday, "Development of a Variable Stiffness and Damping Tunable Vibration Isolator", *Journal of Vibration and Control*, Vol. 11, No. 3, pp. 381–396, 2005.

35. Bonello, P., M. J. Brennan and S. J. Elliott, "Vibration Control Using an Adaptive Tuned Vibration Absorber with a Variable Curvature Stiffness Element", *Smart Materials and Structures*, Vol. 14, No. 5, p. 1055, 2005.

36. Dao, T.-P. and S.-C. Huang, "A Compact Quasi-Zero Stiffness Vibration Isolator Using Flexure-Based Spring Mechanisms Capable of Tunable Stiffness", *International Journal of Mechanical and Mechatronics Engineering*, Vol. 10, No. 8, pp. 1572–1581, 2016.

37. Platus, D. L., "Negative-Stiffness-Mechanism Vibration Isolation Systems", *Vibration Control in Microelectronics, Optics, and Metrology*, Vol. 1619, pp. 44–54, International Society for Optics and Photonics, 1992.

38. Carrella, A., M. Brennan, T. Waters and K. Shin, "On The Design of a High-Static–Low-Dynamic Stiffness Isolator Using Linear Mechanical Springs and Magnets", *Journal of Sound and Vibration*, Vol. 315, No. 3, pp. 712–720, 2008.

39. Wu, W., X. Chen and Y. Shan, "Analysis and Experiment of a Vibration Isolator Using a Novel Magnetic Spring with Negative Stiffness", *Journal of Sound and Vibration*, Vol. 333, No. 13, pp. 2958–2970, 2014.

40. Wang, Y.-C. and R. Lakes, "Extreme Stiffness Systems due to Negative Stiffness Elements", *American Journal of Physics*, Vol. 72, No. 1, pp. 40–50, 2004.

41. Virgin, L. and R. Davis, "Vibration Isolation Using Buckled Struts", *Journal of Sound and Vibration*, Vol. 5, No. 260, pp. 965–973, 2003.

42. Lee, C.-M., V. Goverdovskiy and A. Temnikov, "Design of Springs with "Negative" Stiffness to Improve Vehicle Driver Vibration Isolation", *Journal of Sound and*

Vibration, Vol. 302, No. 4-5, pp. 865–874, 2007.

43. Du, H., W. Li and N. Zhang, "Semi-Active Variable Stiffness Vibration Control of Vehicle Seat Suspension Using an MR Elastomer Isolator", *Smart Materials and Structures*, Vol. 20, No. 10, p. 105003, 2011.

44. Kamesh, D., R. Pandiyan and A. Ghosal, "Passive Vibration Isolation of Reaction Wheel Disturbances Using a Low Frequency Flexible Space Platform", *Journal of Sound and Vibration*, Vol. 331, No. 6, pp. 1310–1330, 2012.

45. Alujević, N., D. Čakmak, H. Wolf and M. Jokić, "Passive and Active Vibration Isolation Systems Using Inerter", *Journal of Sound and Vibration*, Vol. 418, pp. 163–183, 2018.

46. Liu, Y., H. Matsuhisa, H. Utsuno and J. G. Park, "Vibration Isolation by a Variable Stiffness and Damping System", *JSME International Journal Series C Mechanical Systems, Machine Elements and Manufacturing*, Vol. 48, No. 2, pp. 305–310, 2005.

47. Le, T. D. and V. A. D. Nguyen, "Low Frequency Vibration Isolator with Adjustable Configurative Parameter", *International Journal of Mechanical Sciences*, Vol. 134, pp. 224–233, 2017.

48. Blevins, R. D., *Formulas for Natural Frequency and Mode Shape*, RE Krieger Malabar, FL, 1979.

49. Timoshenko, S. P. and J. M. Gere, *Theory of Elastic Stability*, Courier Corporation, 2009.

50. Shaker, F. J., "Effect of Axial Load on Mode Shapes and Frequencies of Beams", *National Aeronautics and Space Administration: Washington, DC*, 1975.

51. Fulcher, B. A., D. W. Shahan, M. R. Haberman, C. Conner Seepersad and P. S. Wilson, "Analytical and Experimental Investigation of Buckled Beams as Negative

Stiffness Elements for Passive Vibration and Shock Isolation Systems", *Journal of Vibration and Acoustics*, Vol. 136, No. 3, 2014.

52. Qiu, J., J. H. Lang and A. H. Slocum, "A Curved-Beam Bistable Mechanism", *Journal of Microelectromechanical Systems*, Vol. 13, No. 2, pp. 137–146, 2004.

53. Gzal, M., M. Groper and O. Gendelman, "Analytical, Experimental and Finite Element Analysis of Elliptical Cross-Section Helical Spring with Small Helix Angle Under Static Load", *International Journal of Mechanical Sciences*, Vol. 130, pp. 476–486, 2017.

54. Wahl, A. M., *Mechanical Springs*, Penton Publishing Company, 1944.

APPENDIX A: TECHNICAL DRAWINGS

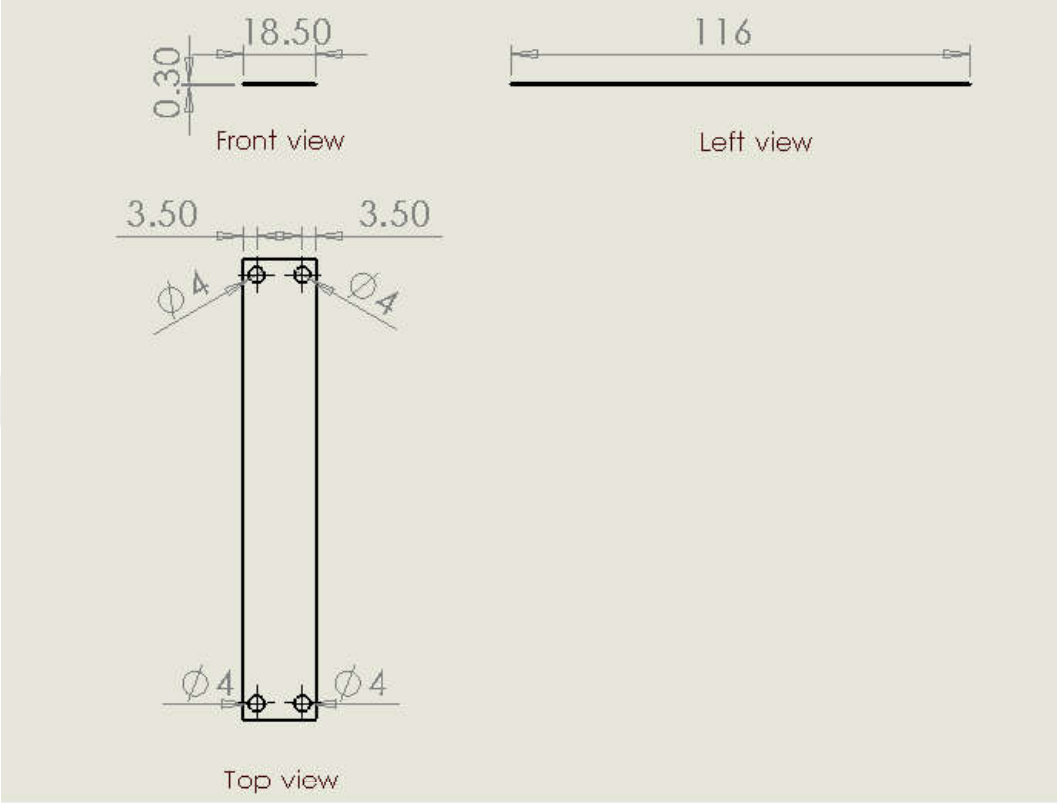


Figure A.1. Axially loaded beams.

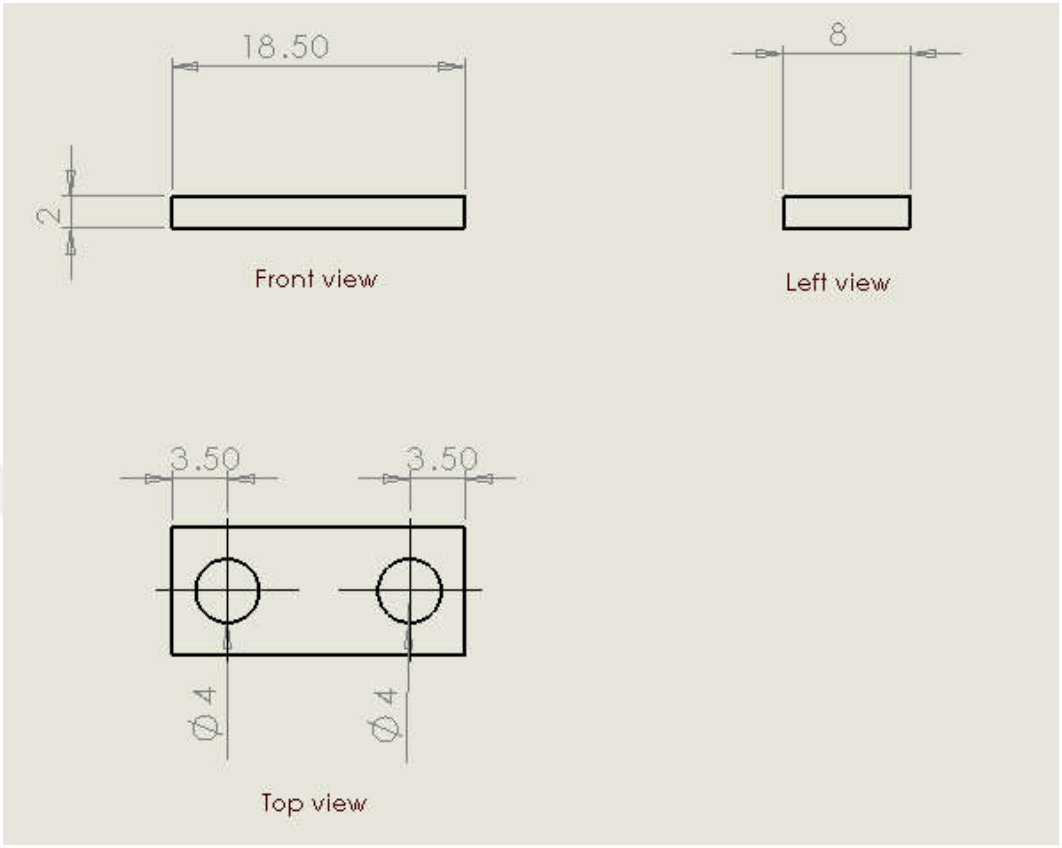


Figure A.2. Spacer between the axially loaded beams.

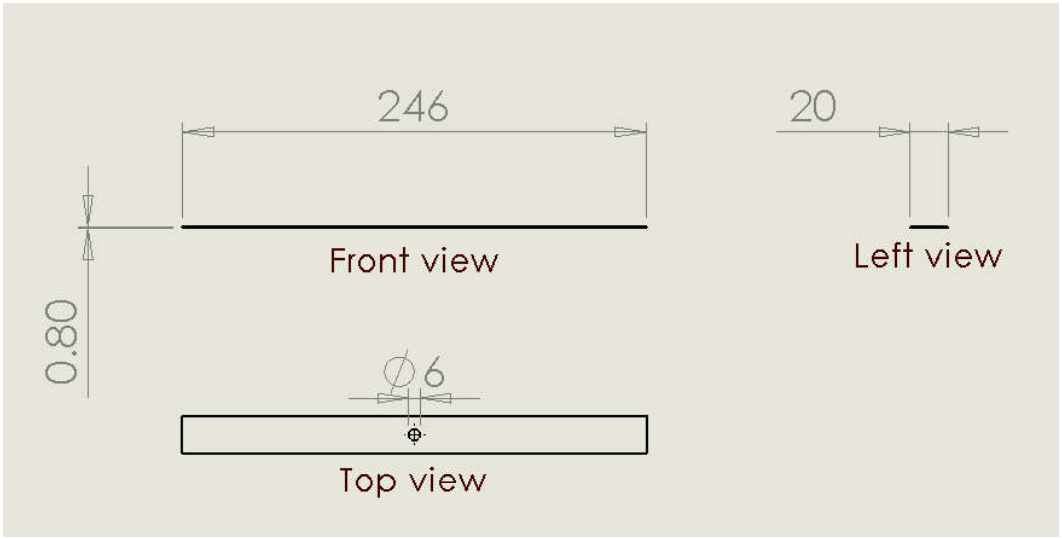


Figure A.3. Negative stiffness element.

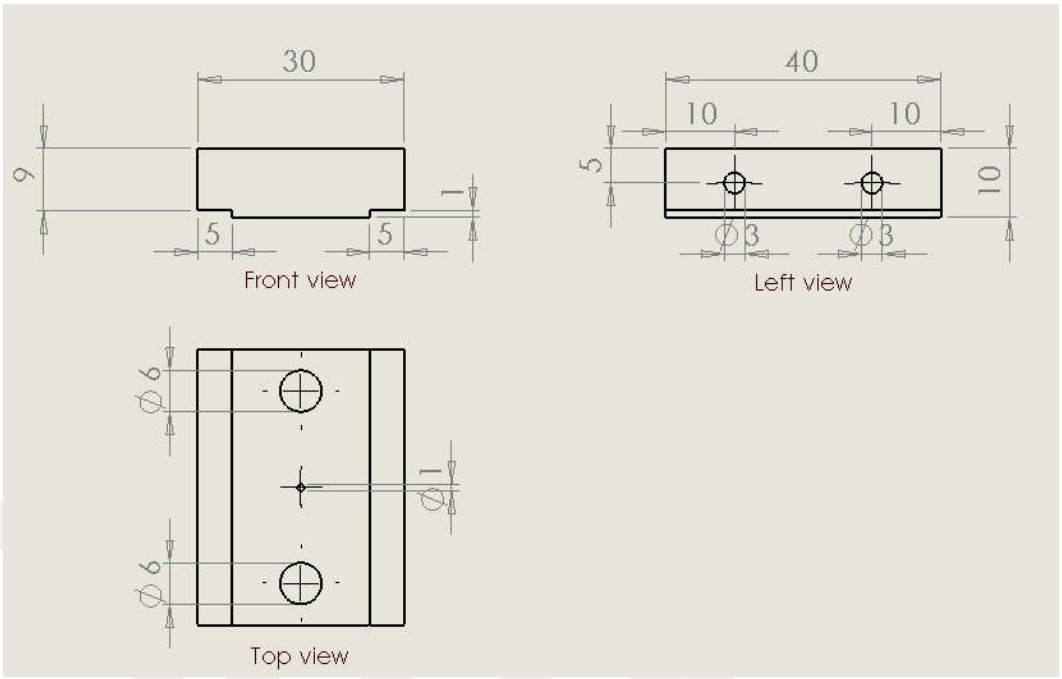


Figure A.4. Part between positive stiffness element and negative stiffness element.

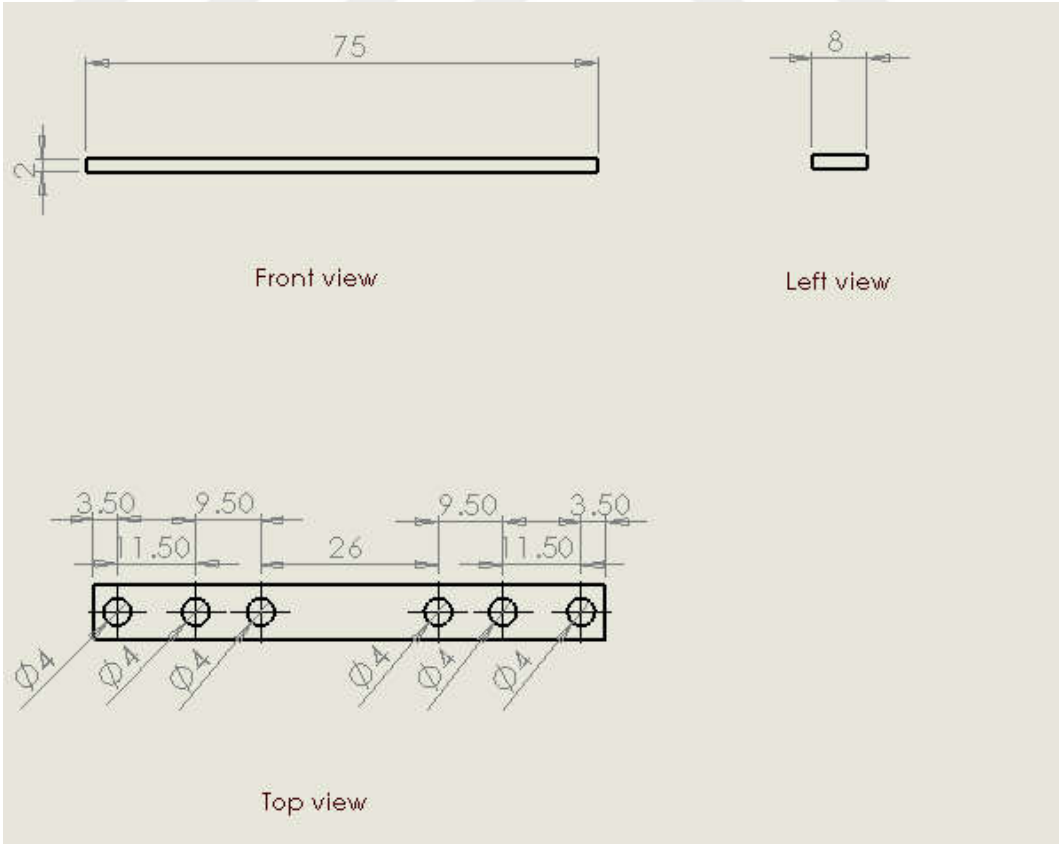


Figure A.5. Top and bottom holders of axially loaded beams.

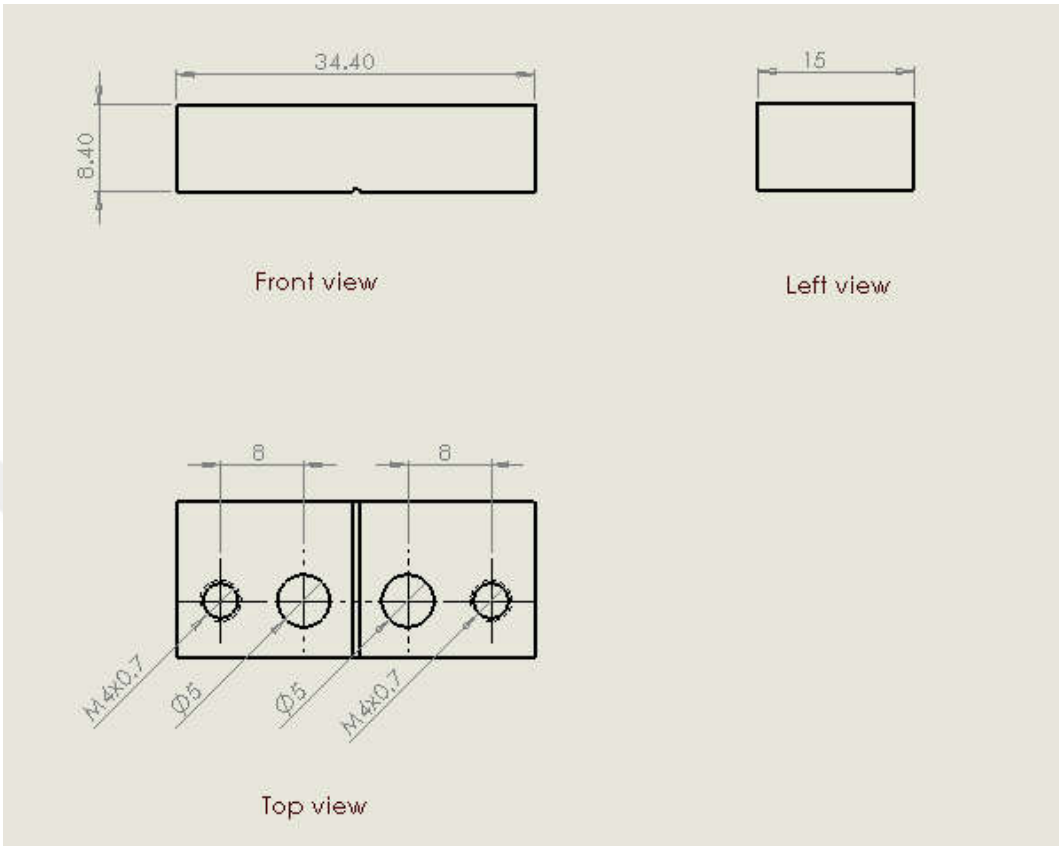


Figure A.6. Wire holder.

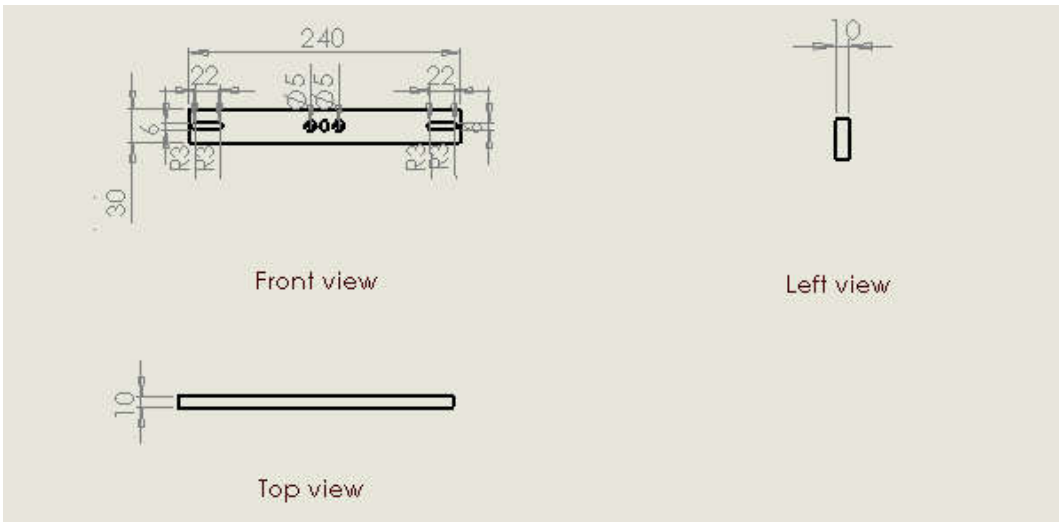


Figure A.7. Fixed frame.

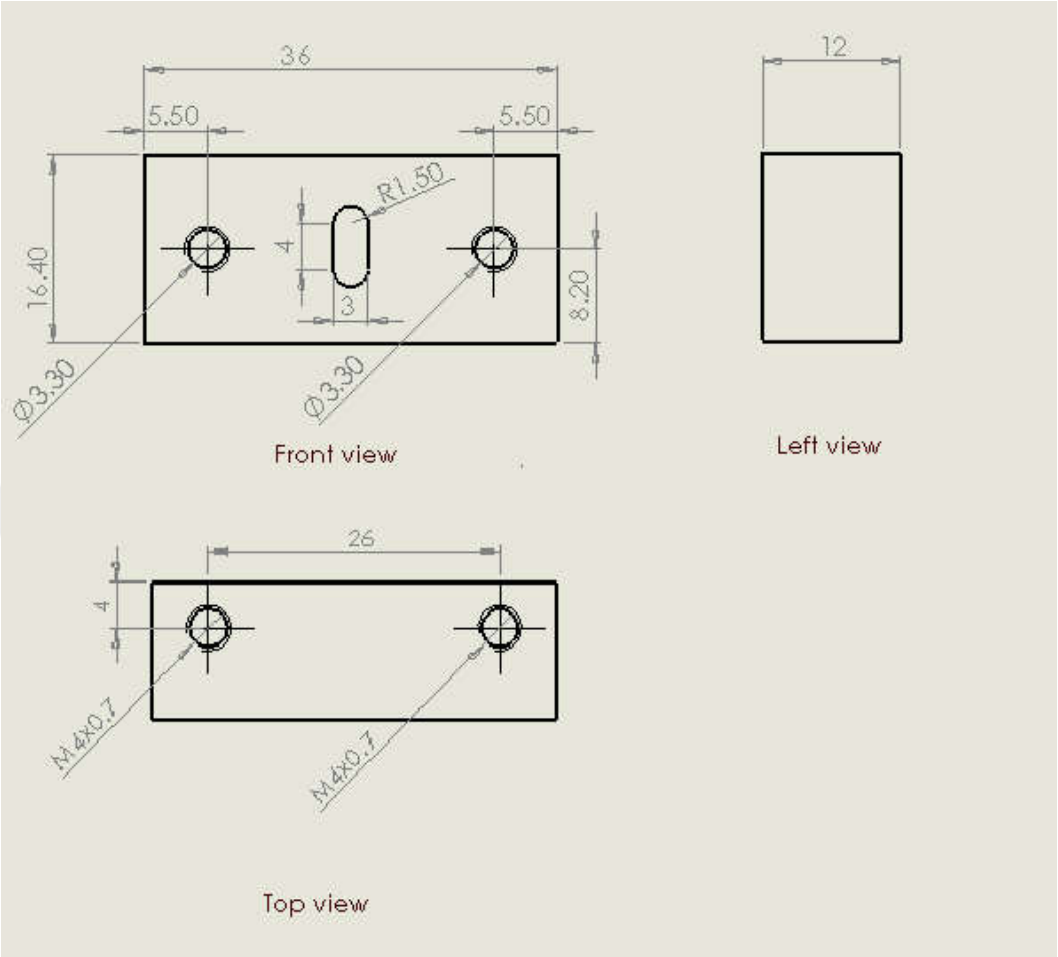


Figure A.8. Connector with elliptical hole.

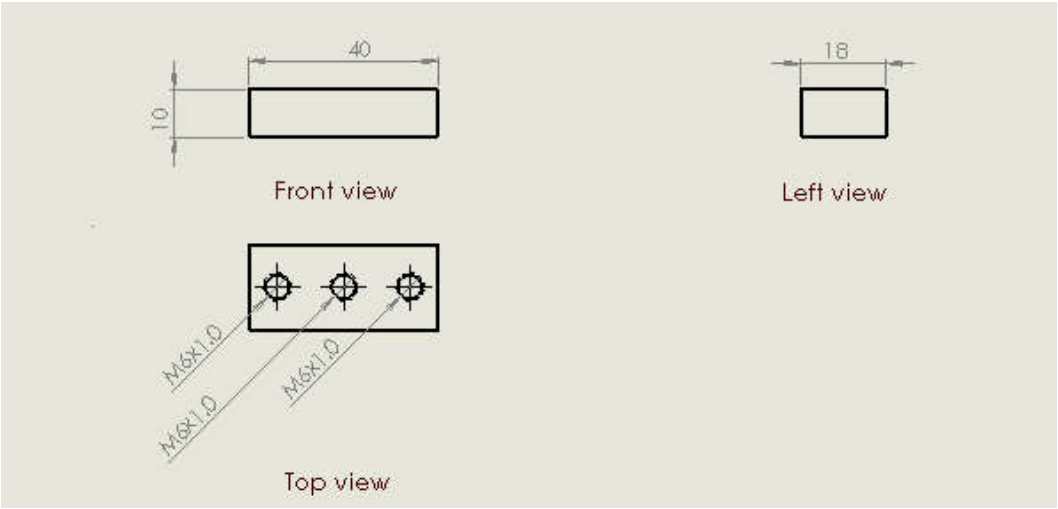


Figure A.9. Side bottom connector pieces.

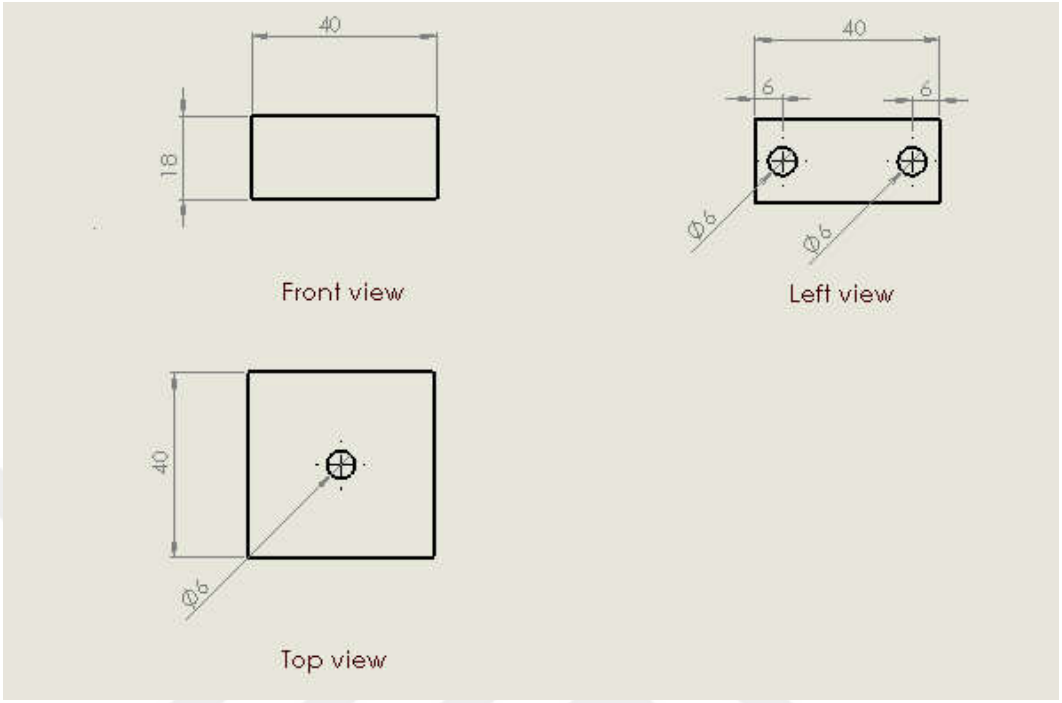


Figure A.10. Side middle pieces.

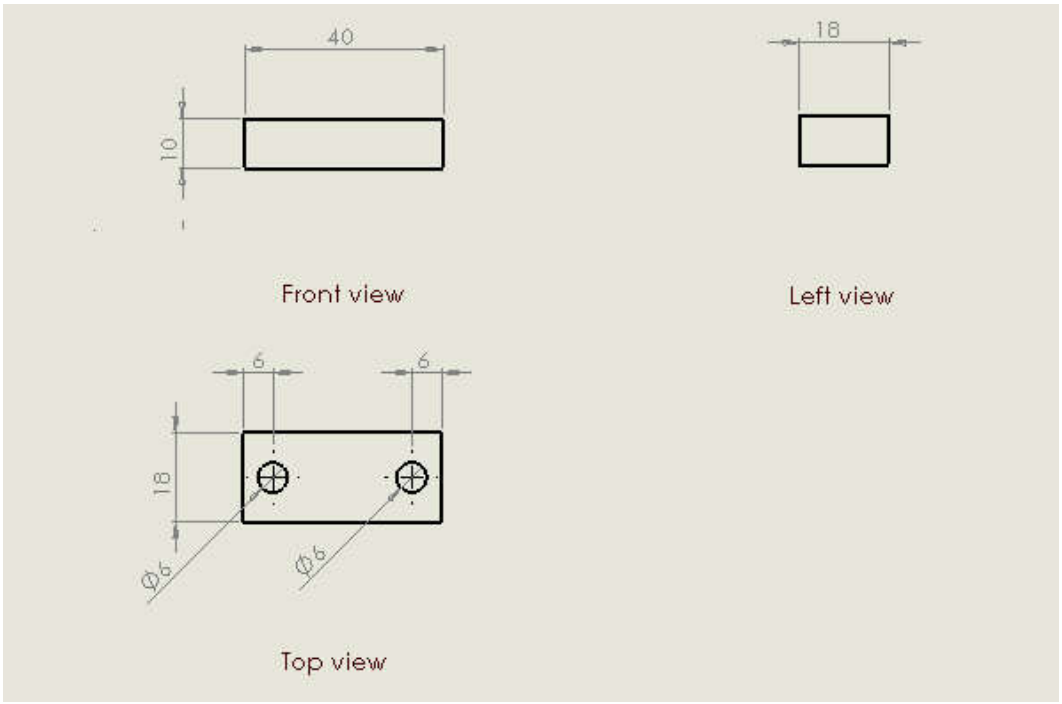


Figure A.11. Side top pieces.

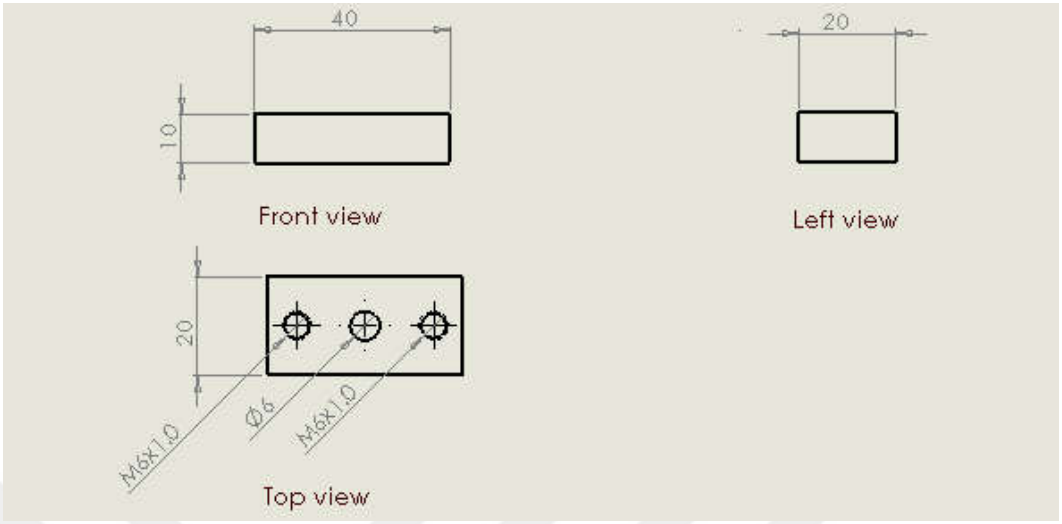


Figure A.12. Center bottom piece.

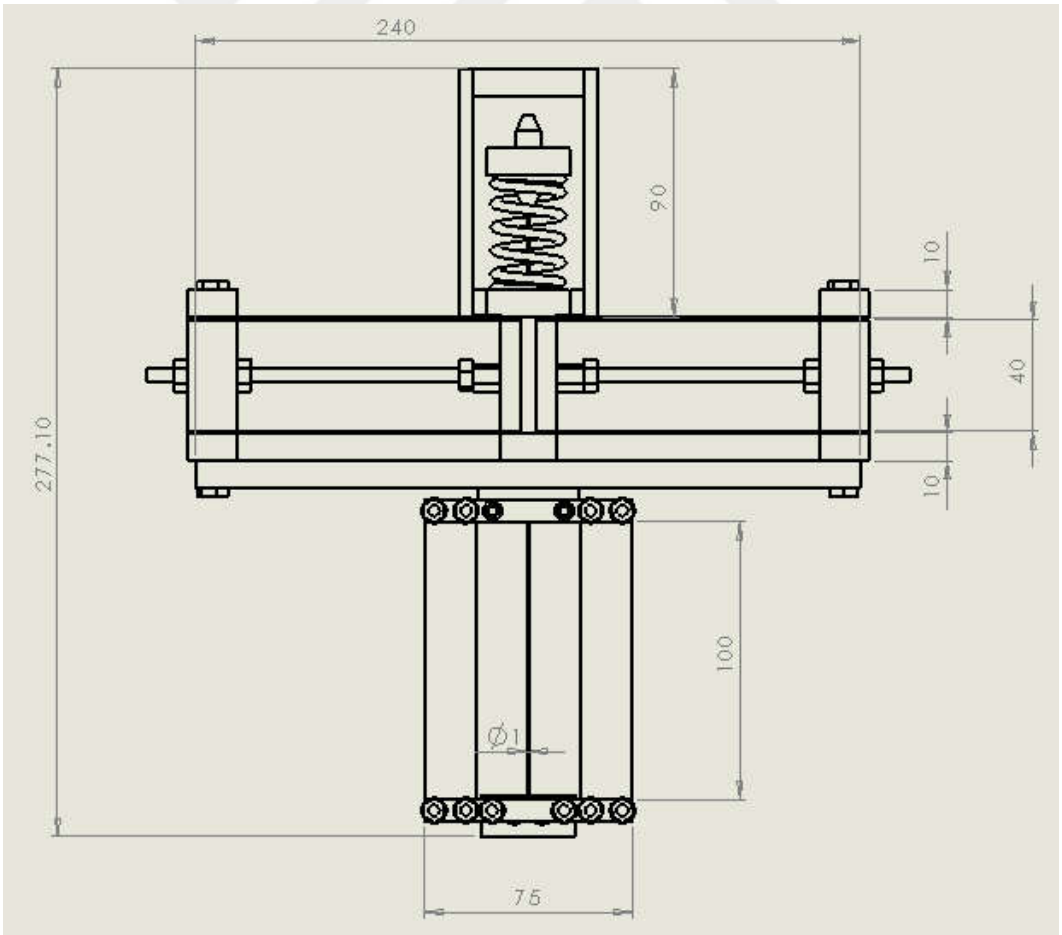


Figure A.13. Front view of final design.

APPENDIX B: COPYRIGHTS

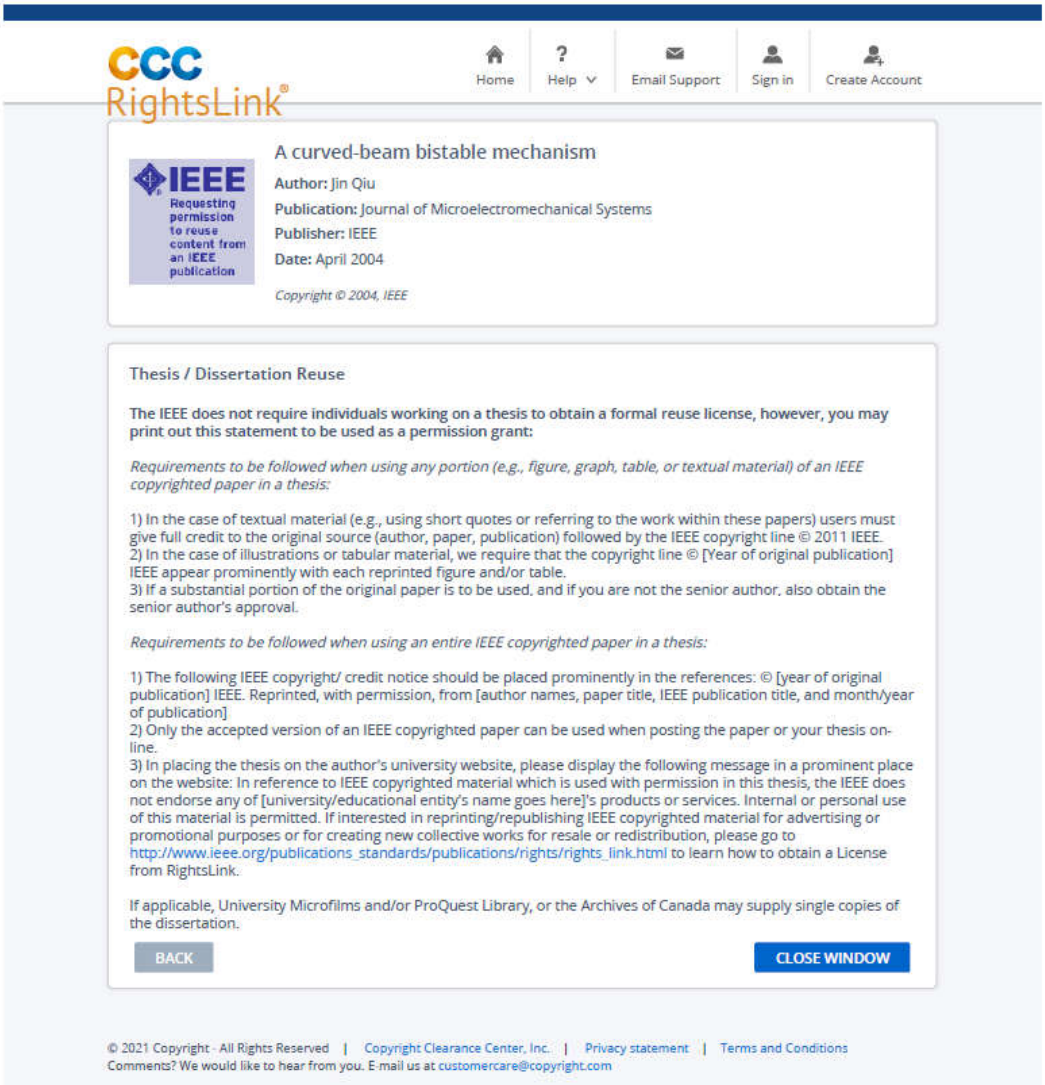


Figure B.1. Copyright 1

ELSEVIER LICENSE
TERMS AND CONDITIONS

Sep 10, 2021

This Agreement between Mr. Sergen Haydin ("You") and Elsevier ("Elsevier") consists of your license details and the terms and conditions provided by Elsevier and Copyright Clearance Center.

License Number	5145511402701
License date	Sep 10, 2021
Licensed Content Publisher	Elsevier
Licensed Content Publication	Journal of Sound and Vibration
Licensed Content Title	Static analysis of a passive vibration isolator with quasi-zero-stiffness characteristic
Licensed Content Author	A. Carrella,M.J. Brennan,T.P. Waters
Licensed Content Date	Apr 3, 2007
Licensed Content Volume	301
Licensed Content Issue	3-5
Licensed Content Pages	12
Start Page	678
End Page	689
Type of Use	reuse in a thesis/dissertation

Figure B.2. Copyright 2

ELSEVIER LICENSE
TERMS AND CONDITIONS

Sep 10, 2021

This Agreement between Mr. Sergen Haydin ("You") and Elsevier ("Elsevier") consists of your license details and the terms and conditions provided by Elsevier and Copyright Clearance Center.

License Number	5145520350233
License date	Sep 10, 2021
Licensed Content Publisher	Elsevier
Licensed Content Publication	Journal of Sound and Vibration
Licensed Content Title	Vibration isolation characteristics of a nonlinear isolator using Euler buckled beam as negative stiffness corrector: A theoretical and experimental study
Licensed Content Author	Xiuchang Huang,Xingtian Liu,Jingya Sun,Zhiyi Zhang,Hongxing Hua
Licensed Content Date	Feb 14, 2014
Licensed Content Volume	333
Licensed Content Issue	4
Licensed Content Pages	17
Start Page	1132
End Page	1148
Type of Use	reuse in a thesis/dissertation

Figure B.3. Copyright 3